JAERI-M
8625

IAEA INTOR WORKSHOP REPORT, GROUP 12
—— START-UP, BURN AND SHUTDOWN ——

January 1980

Fusion Research and Development Center

日本原子力研究所
Japan Atomic Energy Research Institute

この報告書は，日本原子力研究所がJAERI-Mレポートとして，不定期に刊行している研究報告書です．入手，複製などのお問合わせは，日本原子力研究所技術情報部（茨城県那珂郡東海村）あて，お申しこしください．

JAERI-M reports, issued irregularly, describe the results of research works carried out in JAERI. Inquiries about the availability of reports and their reproduction should be addressed to Division of Technical Information, Japan Atomic Energy Research Institute, Tokai-mura, Naka-gun, Ibaraki-ken, Japan.

JAERI-M 8625

IAEA INTOR Workshop Report, Group 12

—— Start-up, Burn and Shutdown ——

Fusion Research and Development Center,
Tokai Research Establishment, JAERI

(Received December 12, 1979)

This report gives the material for the IAEA INTOR Workshop for data base discussion in Group 12, Start-up, Burn and Shutdown. Number of problem areas from the generation of a plasma to the termination of the discharge are covered, which should be assessed to develop a scenario for sustaining a plasma for the whole duration of a pulse. The reactor relevant burn pulse is also assessed.

Key words : INTOR Tokamak Reactor, Start-up, Burn, Shutdown, Control

Prepared by : Tatsuzo TONE (Group leader),
Masao KASAI*1, Hiroshi KISHIMOTO, Koichi MAKI*2
Naoyuki MIYA*3, Ryuichi SHIMADA, Kichiro SHINYA*4,
Masayoshi SUGIHARA, Teruhiko TAZIMA, Hidetoshi YOSHIDA

---

*1 On leave from Mitsubishi Atomic Power Industries Inc.
*2 On leave from Hitachi, Ltd.
*3 Scholarship fellow from Nihon University
*4 On leave from Tokyo Shibaura Electric Co., Ltd.

JAERI－M 8625

IAEA INTORワークショップ検討報告書・グループ12
── プラズマの立上げ，燃料および停止 ──

日本原子力研究所東海研究所
核融合研究開発推進センター

（1979年12月12日受理）

このレポートは，INTOR（国際協力トカマク炉）のプラズマの検討の一環として行ったプラズマの立上げ，燃焼および停止に関するデータベースの評価をまとめたものである。

執筆者　東稔達三（グループリーダー）・笠井雅夫[*1]・岸本　浩
真木紘一[*2]・宮　直之[*3]・嶋田隆一・新谷吉郎[*4]
杉原正芳・田島輝彦・吉田英俊

＊1）外来研究員：三菱原子力工業㈱
＊2）外来研究員：日立製作所
＊3）特別研究生：日本大学
＊4）外来研究員：東京芝浦電気㈱

CONTENTS

(edited by T. Tone)

目　　次

1. INTRODUCTION

Operating the INTOR plasma properly during start-up, burn and shutdown phases requires the establishment of reactor relevant physics and technologies in both software and hardware fields. The scenario for these phases largely affects a reactor design. Complete solutions for all the issues related to the three phases, however, would not necessarily be obtainable before INTOR operation, since the time schedule for decision is tight and some of them are really tested in INTOR for the first time. As a result, it is inevitable that some part of the scenario is at present highly speculative.

Among the three phases there exists a rich data base for start-up and shutdown on present-day devices and the experiences of design and technology for the larger devices under construction (TFTR, JT-60, JET), which would enable us to reasonably extrapolate most of them to the next step, INTOR. The β valve required for INTOR is considerably high ($5 \sim 6\%$) when compared with the present-day value. A start-up scenario for obtaining such a high, stable β value with the control of current profile, fueling, heating and impurities is one of the most important issues. The required β value is at present relatively speculative, but the value of this degree is thought to be a reasonable physics target of INTOR in view of the present-day experimental results and theoretical analyses.

On the other hand, requirements for the long burn phase in INTOR provide an entirely new situation in physics and technology. The burn control of self-ignition plasma and the ash exhaust are the most critical issues in the burn phase. Information on alpha heating will be available from TFTR and JET. However, no complete solution for burn control and ash exhaust would be established before INTOR. The real test of the two issues should be thought to be carried out in INTOR itself. In order to make the uncertainty and risk involved in the present speculation as small as possible, extensive research and development should be done to obtain the confirmative information with the devices available before INTOR.

For the shutdown phase, the techniques to terminate the discharge and recover the poloidal magnetic field energy without inducing plasma current disruptions must be developed. Confirmative information on this issue is expected to be available before INTOR operation, since the experiments on the large tokamaks (TFTR, JT-60, JET) will provide

a useful data base.

The following are among the R and D requirements related to start-up, burn and shutdown.

· Startup techniques of attaining a desirable current profile and low q_a for a large plasma.

· The plasma confinement mechanism at current initiation for a large plasma should be elucidated and the maximum rate of current rise should be reduced as low as possible, at least less than 1 MA/s, in view of SCM design.

· Controllability of ion energy loss by a variable field ripple and engineering feasibility of ripple coils.

· Fueling technique of attaining a desirable plasma profile by gas puffing and plasma expansion technique during startup phase for a large plasma.

· Pellet injection technique being capable of the deep penetration of fuel particles to a plasma center for a large plasma.

Main problem areas related to start-up, burn and shutdown are treated also in the other group reports, i.e., energy and particle confinement (Group 1)[1], impurity control, fueling and exhaust (Group 3)[2], heating (Group 4)[3], stability control (Group 11)[4] and power supply and transfer (Group 8)[5], respectively. This report attempts to cover the items given in the INTOR Workshop, but the items directly corresponding to the other group reports are briefly described, when the details are given in the respective group reports.

References

1) JAERI-M 8621, (Jan., 1980)
2) JAERI-M 8622, (Jan., 1980)
3) JAERI-M 8623, (Jan., 1980)
4) JAERI-M 8624, (Jan., 1980)
5) JAERI-M 8511, (Oct., 1979).

2. START-UP

The start-up of the INTOR is treated by dividing it into three typical time phases:

(i) Gas breakdown and current initiation

(ii) Ohmic heating with continuous plasma minor radius expansion and current increase

(iii) Additional heating with energetic neutral beam injection and fueling to the self-ignition state.

The start-up scenario is shown schematically in Fig.1.

2.1 Gas Breakdown and Current Initiation at Low Voltage

Computer simulations on INTOR current initiation at low voltage ($\lesssim$ 50 V) have been carried out more precisely than those reported in Session 2 (Appendix A). The one-turn voltage of 50 V corresponds to E $\simeq$ 0.015 V/cm, and E/P is about 150 V/cm·torr assuming initial filling pressure of 10^{-4} torr. Runaway electrons do not play an important role in these conditions. Due to strong toroidal electric field, electrons gain high energy (up to $\sim 10^{7}$ cm/sec) and move along toroidal magnetic field with negligible thermal speed. Both axial (B_Z) and radial (B_R) poloidal magnetic field can cause electron to escape to wall because these error fields deform toroidal magnetic field and the field lines intersect the chamber wall. Electric drift due to $\tilde{E}_{toroidal} \times \tilde{B}_{poloidal}$ and curvature drift can also cause electron loss, but the effect of these drifts is an order of magnitude smaller than orbit loss.

1) Effect of non-axisymmetric magnetic field

Non-axisymmetric magnetic field is produced by miss-alignment of toroidal and/or poloidal field coils and is generally uni-directional (n=1), i.e. electrons drift in the opposite direction when they pass the opposite side of the torus. Therefore electrons drift very little when averaged in the toroidal direction if electrons can rotate many times around the torus. If non-axisymmetric field has a high mode number ($n \geq 2$), averaging process can be done more effectively. Therefore non-axisymmetric magnetic field hardly causes electrons to escape by orbit loss or electric drift.

2) Results of simulations

Figure 2 shows the time evolution of the plasma current with corresponding voltage forms. The electron density is shown in Fig. 3. These figures show that one-turn voltage lower than 20 V cannot produce the initial plasma. Figure 4 shows the applied voltage which cause the breakdown in the same time lag as a function of filling pressure. Breakdown time lag is defined as an interval between the time of current interruption of the transformer coils and that at which the poloidal magnetic field produced by plasma current overcomes the error field. Figure 5 shows overall time evolution of various quantities in the case of applied voltage of 50 V and error field of 60 G. Initial electron current density is an important factor to breakdown the filling gas successfully. In the case of INTOR, fortunately almost all structures inside the shield are activated, so the gas can be pre-ionized by the radiation.

It is concluded that INTOR current initiation can be performed successfully at low voltage (< 50 V) in the wide range of filling pressure (2×10^{-5} - 10^{-4} torr) if an error field can be suppressed below 60 G.

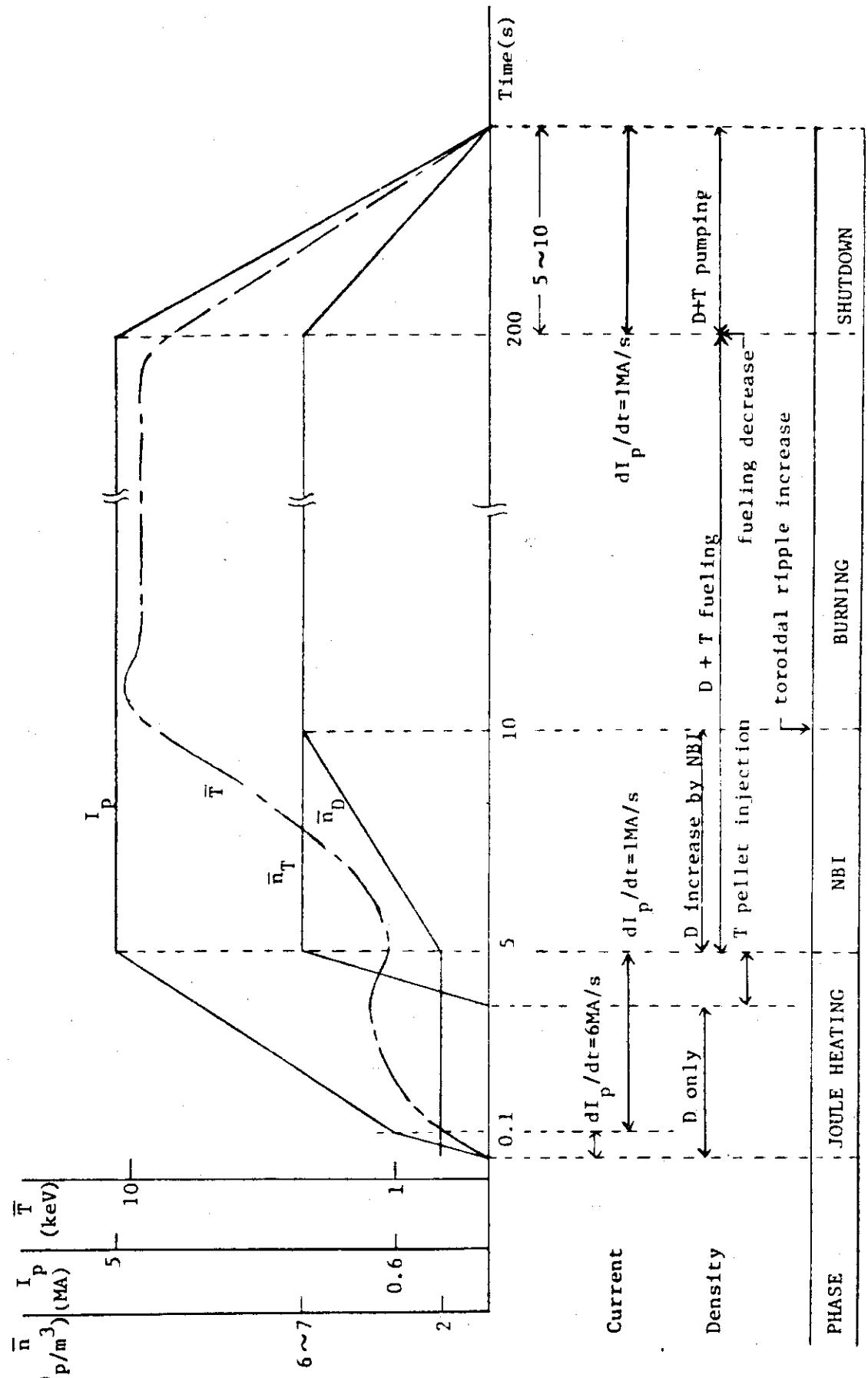

Fig. 1 Schematical drawing of the start up, burn and shut down scenario

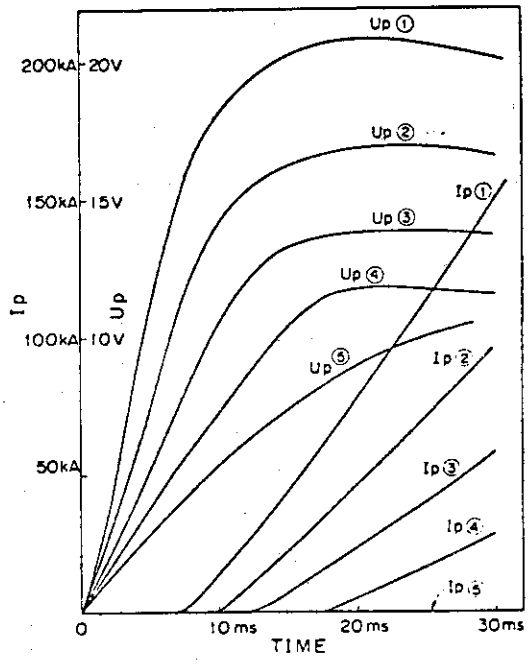

Fig. 2 Time evolution of plasma current and oneturn voltage

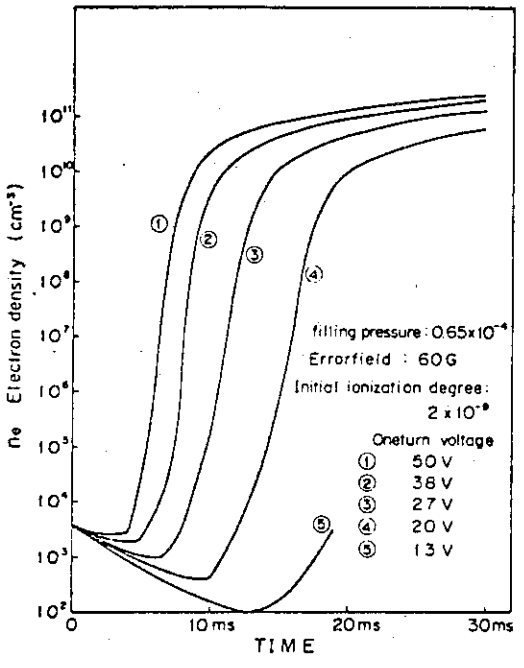

Fig. 3 Time evolution electron density

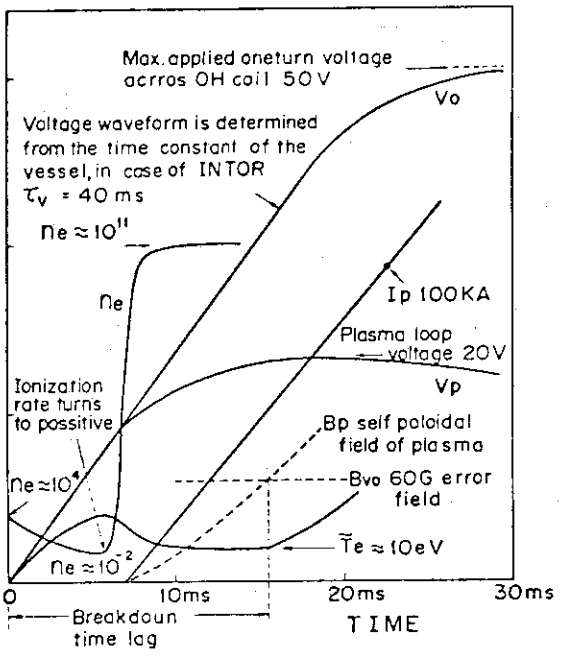

Fig. 5 Overall time evolution of various quantities relating breakdown phenomena

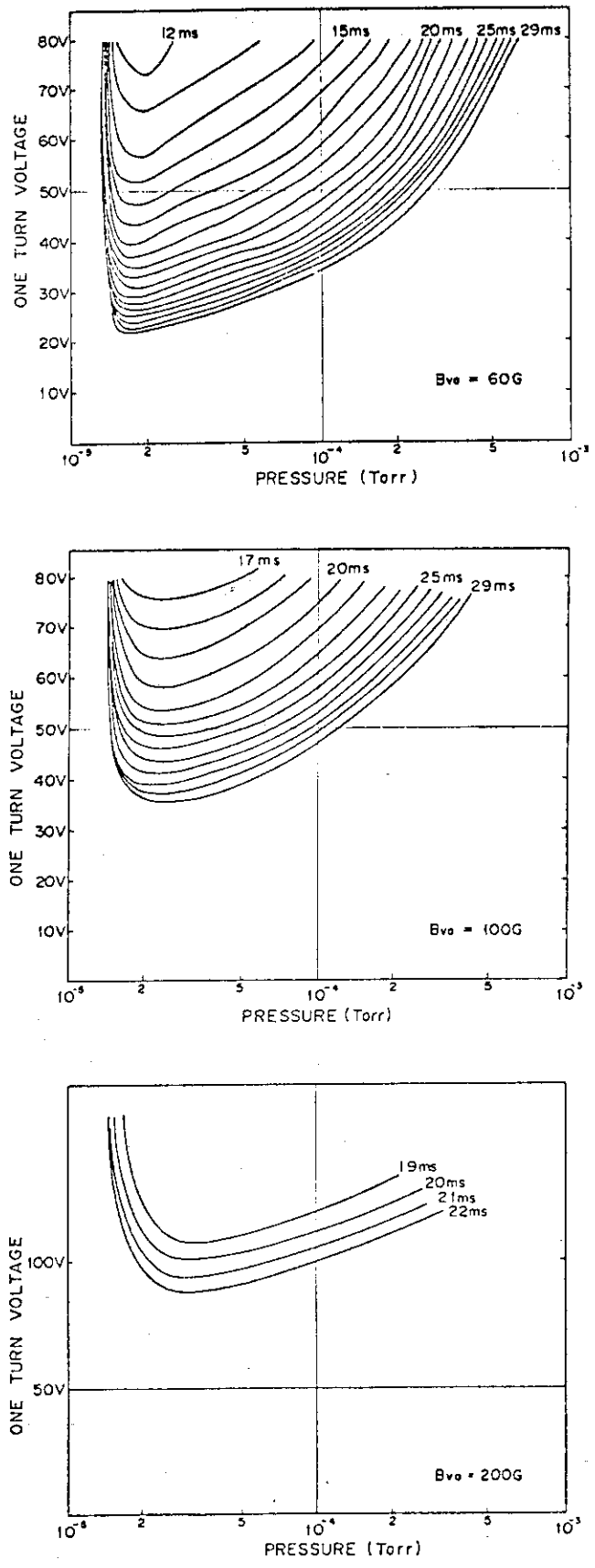

Fig. 4 Possible breakdown region with breakdown time lags as parameters for three cases of the error vertical field

2.2 Plasma Current Rise

1) Minor radius expansion

Empirical scaling laws of achievable mean desities $\bar{n}$[1),2)] (Fig.1) show that $\bar{n}$ is a function of joule input power density. From the technological restrictions, INTOR should have a current rise time longer than several seconds. Therefore it may be hard to obtain a suitable density higher than $10^{19}/m^3$ for avoiding runaway discharges, since joule input power density is very small in such a slow current rise phase. Minor radius expansion is one of the potential methods to keep high joule input density during the current rise phase.

A strong skin effect in the current density distribution occurs in a computer simulation of a reactor plasma because of its large plasma radius. The joule heating is not so effective as in the cases without skin effect, since the most of joule heating power is deposited in the skin region where the energy losses of the electrons are very large, and consequently the electron temperature becomes nearly equal to the ion temperature. The joule input power per unit volume in a large tokamak becomes small on a scaling of $1/R^2$. Furthermore, a strong skin effect of the plasma current tends to make the plasma MHD-unstable.

The current density distribution dose not change so much in a keV plasma because of its long skin time, even in the case that the temperature increases from a keV to multi-keV by additional heating. Therefore, it is important to attain a desirable distribution of current density in a joule heating phase by using, for example, minor radius expansion. However, it is necessary to control the plasma density by a method such as gas puffing in the minor radius expansion phase. It is because high filling pressure (e.g. 10^{-4}Torr) will cause excessive density and blow off the plasma in the very initial phase, since most of the neutral gases will flow into the plasma within several milli-seconds. Therefore filling pressure should be low (e.g. 10^{-5}Torr). Consequently, we should feed fuels with volume expansion to avoid the decrease of the density.

Full understanding and the necessary information on an adequate current rise scenario will be obtained through the experiment of JT-60, since JT-60 is designed to be able to test the plasma expansion during current rise.

2) Scheme for current rise

The plasma current rise of INTOR is performed in the following ways. Evolution of a plasma minor radius is made by continuous expansion of the separatrix defining a plasma surface by appropriate control of the poloidal field coil currents. Rate of plasma current rise must be so small that both electric power required for the poloidal field coils and heat dissipation due to fast change of the poloidal magnetic field in the super-conducting toroidal field coils can be lowered to an adequate value which is technologically tolerable. This raises reality of a fusion reactor.

3) Effective use of input power

To heat the plasma effectively, attention must be paid to the energy balance. During breakdown and current initiation, energy is supplied from induced electric field and is lost by escapes of charged particles due to magnetic field irregularities. Magnetic field leakage from the poloidal field coils into the plasma region can be reduced to about 10 gauss in the design of INTOR. In the succeeding ohmic heating, sufficient power input into the plasma is expected at low q_a discharges, so plasma current and minor radius must be increased in such a way that q_a remains almost constant to the final value.

4) Ohmic heating phase

In a large scale tokamak, ratio of energy loss to ohmic power input decreases, therefore the rate of plasma current rise is reduced to about 1 MA/sec in the INTOR size except for preceding breakdown and current initiation phase.

Figure 2 shows the rate of plasma current build-up obtained through the various experiments in typical tokamak devices[3]. The results can be easily extrapolated to a INTOR size plasma, and it seems to be reasonable to set 1 MA/s current rise. From the point of view of SCM design it is desirable to raise the plasma current slowly in order to decrease heat load to superconducting magnets. The value of 1 MA/s would be a trade-off for physics and technology. In the fast rise phase up to 0.6 MA in 0.1 sec including breakdown of filling gas, the plasma current is increased more rapidly to pass through the poor energy balance region in a short time.

Detailed evolutions of plasma current is shown in the report of Group 8.[4)]

(a) Minor radius expansion

Safety factor of a tokamak plasma is expressed as

$$q_a = \frac{a^* B_t}{R B_p} = \frac{2\pi B_t}{\mu_0 R} \quad \frac{a^2}{I_p} \quad \frac{1+\kappa^2}{2} \quad .$$

Safety factor q_a should remain almost constant during ohmic heating as the value in the stationary burn phase, i.e. plasma current must increase with its density unchanged, because q_a is inversely proportional to the plasma current density I_p/a^2.

If the plasma current increases with constant rate, plasma minor radius, a, should increase in proportion to the square root of time. Plasma can be expanded by defining its boundary with fast movable limiter or separatrix formed by magnetic field interaction of plasma current with poloidal divertor current.

Fast movable limiter is abandoned because of the following reasons.

(a) Intolerable heat load.

(b) Impurity efflux.

(c) Mechanical complexity.

Bundle divertor does not seem to be attractive for the start-up, because surface defining effect is not expected so much.

(b) Power input during ohmic heating

Plasma resistance during ohmic heating has a proportionality given by

$$R_p \propto \kappa^{-1} a^{-2} T^{-3/2} \quad .$$

Resistive drop of a ohmic-heated plasma is

$$V_p = R_p I_p \propto \kappa^{-1} a^{-2} T^{-3/2} I_p \quad .$$

When we raise the plasma current with keeping almost constant $q_a (=(1+\kappa^2)\frac{a^2}{I_p})$, the electric power input into plasma during ohmic heating is

$$P_e = V_p I_p \propto \frac{(1+\kappa^2)^2}{\kappa} \quad a^2 T^{-3/2} q_a^{-2} \quad .$$

Hence the smaller the safety factor is, the more the input power is.

(c) Start time of neutral beam injection

Neutral beam injection is started after the plasma current has fully developed to aim at the followings.

(a) Effective use of injection power at the current flat-top at which energy is confined more effectively.

(b) To avoid over-dense plasma due to fuel injection effect of NBI.

(c) To lower heat load into the first wall along scrape-off layer of the plasma during plasma expansion.

(d) To lower the fraction of the injected beam power which is lost by passing through the plasma.

(e) To avoid current peaking at the plasma center.

(d) Control of the plasma shape during start-up

Final shape of the INTOR plasma is shown in Fig. 3 for both cases with and without divertor. Plasma parameters are

$n = 1.2 \times 10^{20}$ ions/m^3, $\bar{T} = 10$ keV, $I_p = 4.7$ MA, $\beta_p = 2.6$,

$a_p = 1.2$ m, $R_p = 5.0$ m, $\kappa = 1.5$, and $\Delta = 0.4$.

Magnetic field configuration by external conductors are shown in Fig. 4. Figure 5 shows the arrangement of poloidal field coils. Poloidal magnetic field and the n-index at the plasma center are

$$B_v = 0.41 \text{ T, and } n = -1.25$$

respectively. (The results for these parameters were presented at Session 2. For Session 3 the values of β_p and the plasma triangularity, Δ have been slightly changed to 2.5 and 0.3, respectively.)

Details of the control method including the time evolution of the multipole field components of the equilibrium magnetic field and the effect of the plasma triangularity are described in the report of Group 11.[5)]

References

1) S. Konoshima, et al. : J. Nuclear Materials 76 & 77 (1979) 581.

2) L.A. Bery, et al. : Proc. 6th Int. Conf. Plasma Physics and Controlled Nuclear Fusion Research, Berchtesgarden (1976) I, IAEA, Vienna (1977) 49.

3) H. Kishimoto : private communication.

4) JAERI-M 8511 (1979)

5) JAERI-M 8624 (1980)

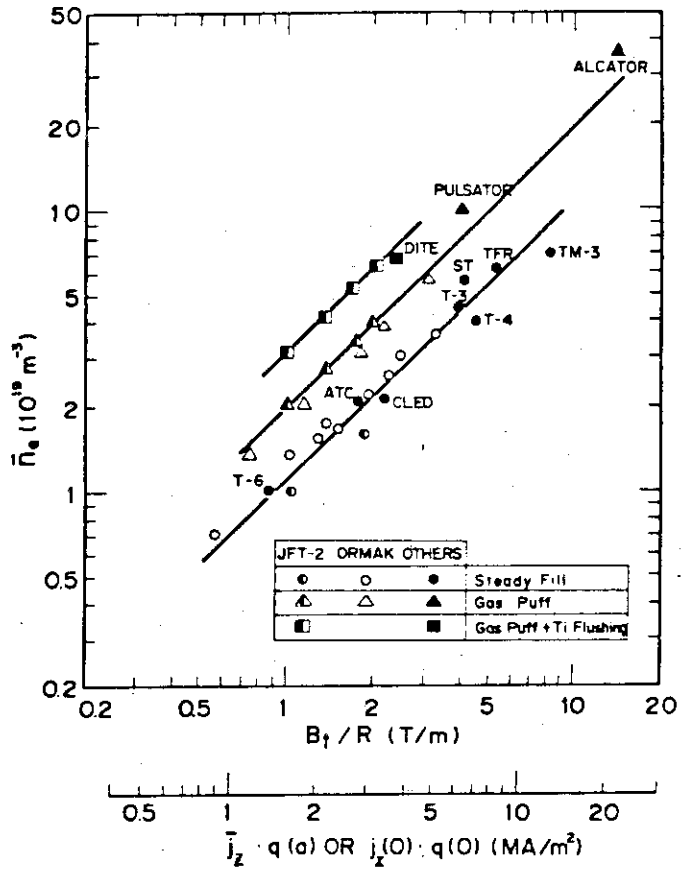

Fig. 1 Scaling law of mean electron densities.
B_t: toroidal magnetic field, R: major radius,
j_z: toroidal plasma current density,
q: safety factor.

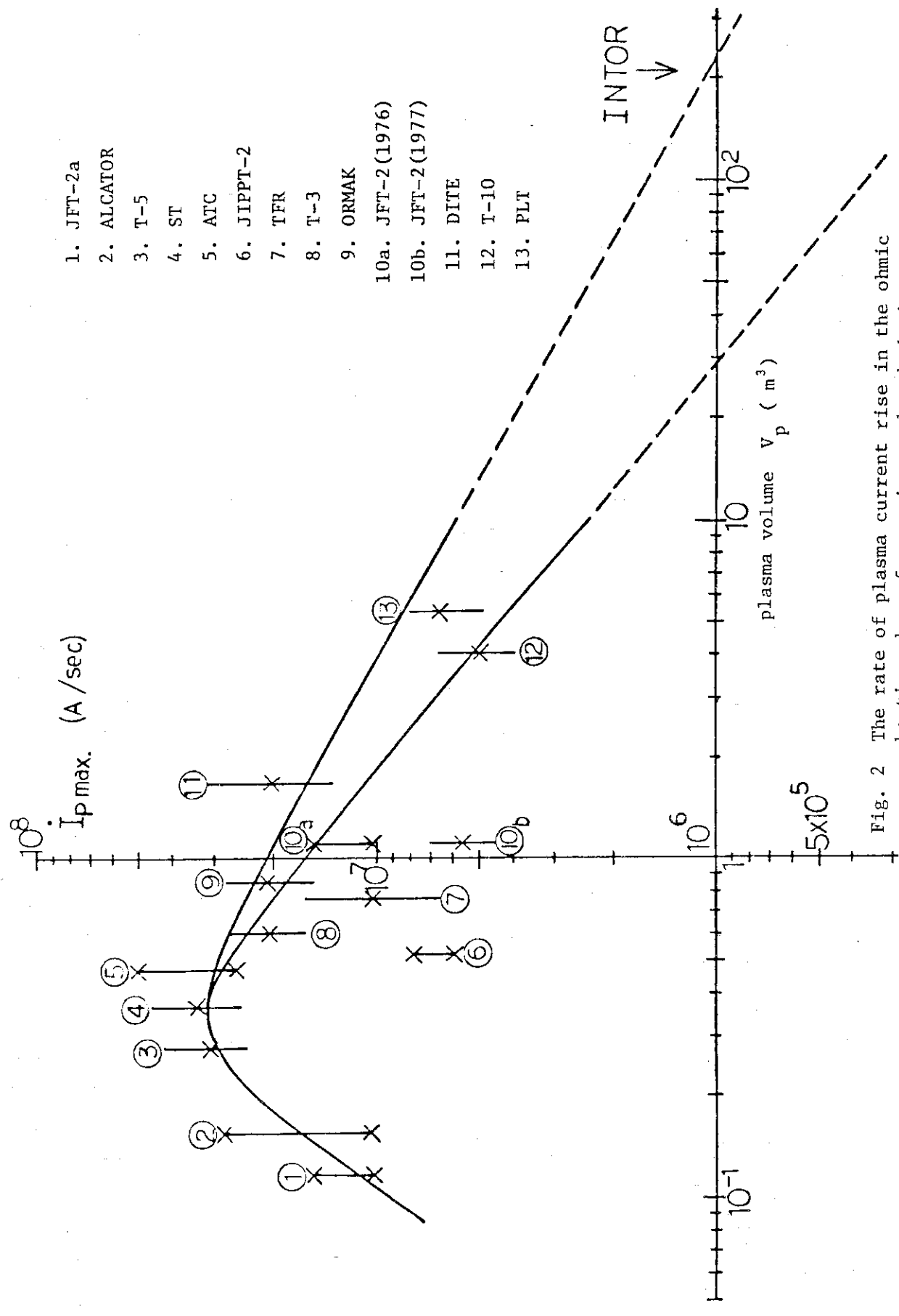

Fig. 2 The rate of plasma current rise in the ohmic heating phase for various tokamak devices

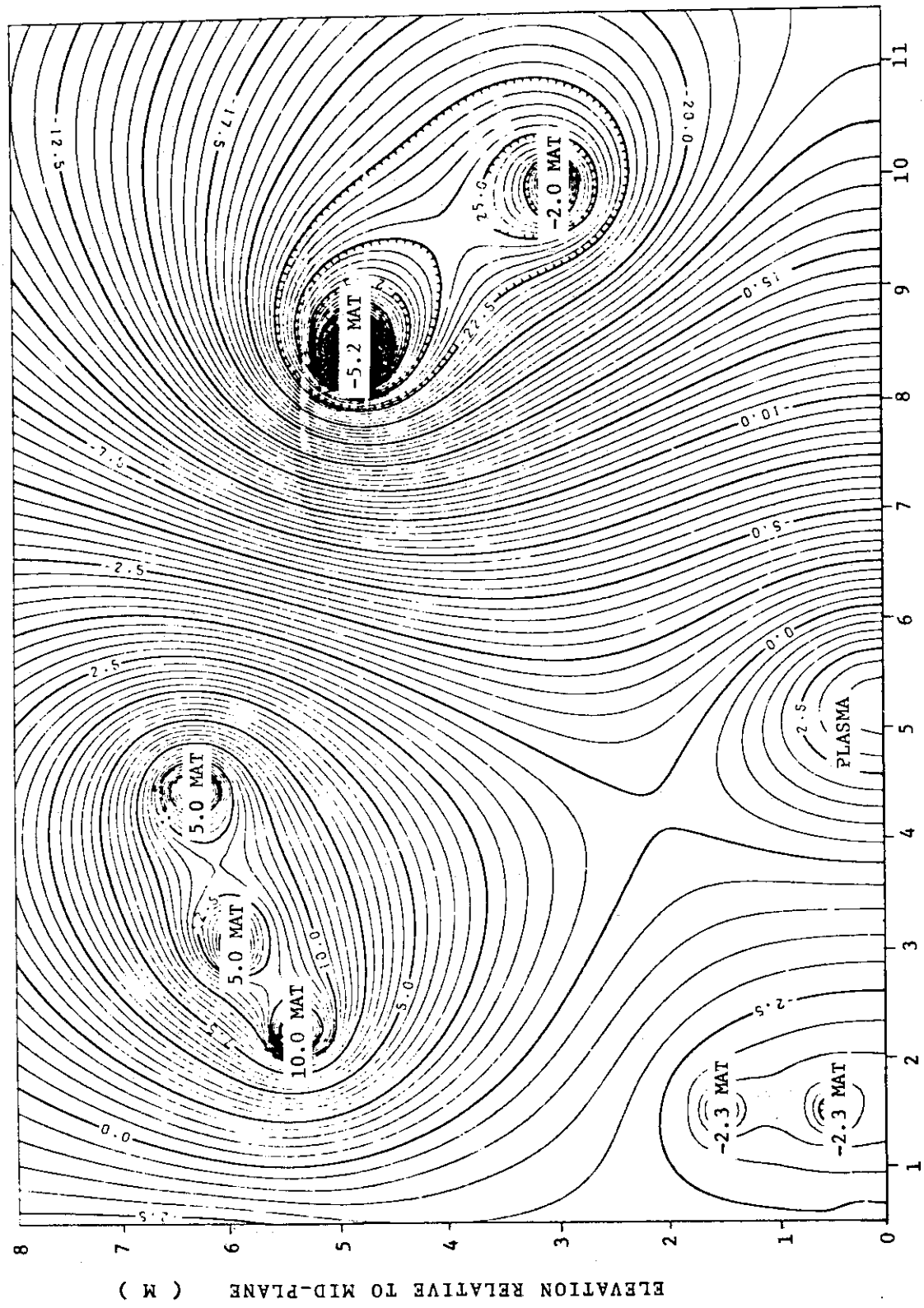

Fig. 3(a) Free boundary equilibrium of INTOR plasma with divertor

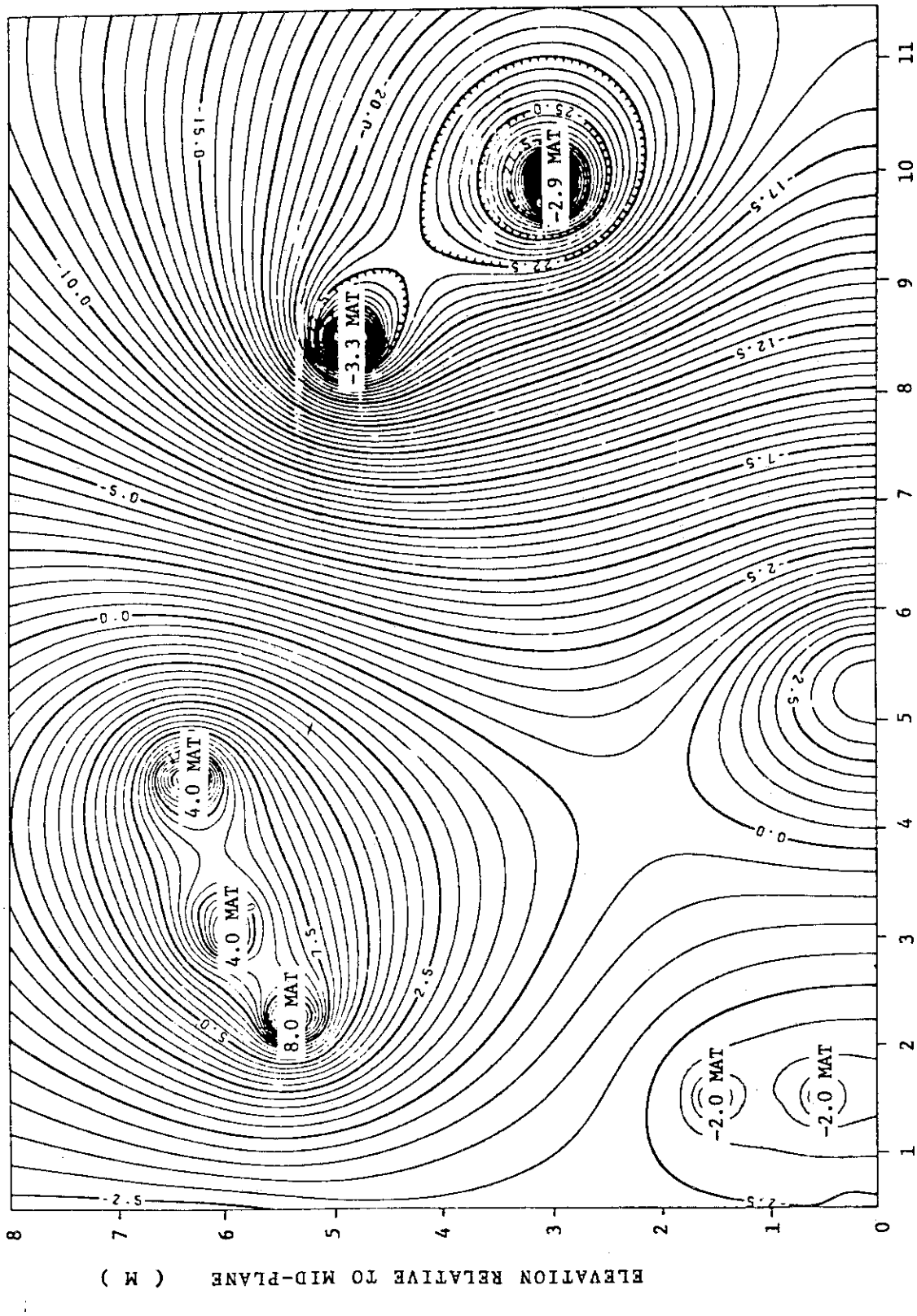

Fig. 3(b) Free boundary equilibrium of INTOR plasma without divertor

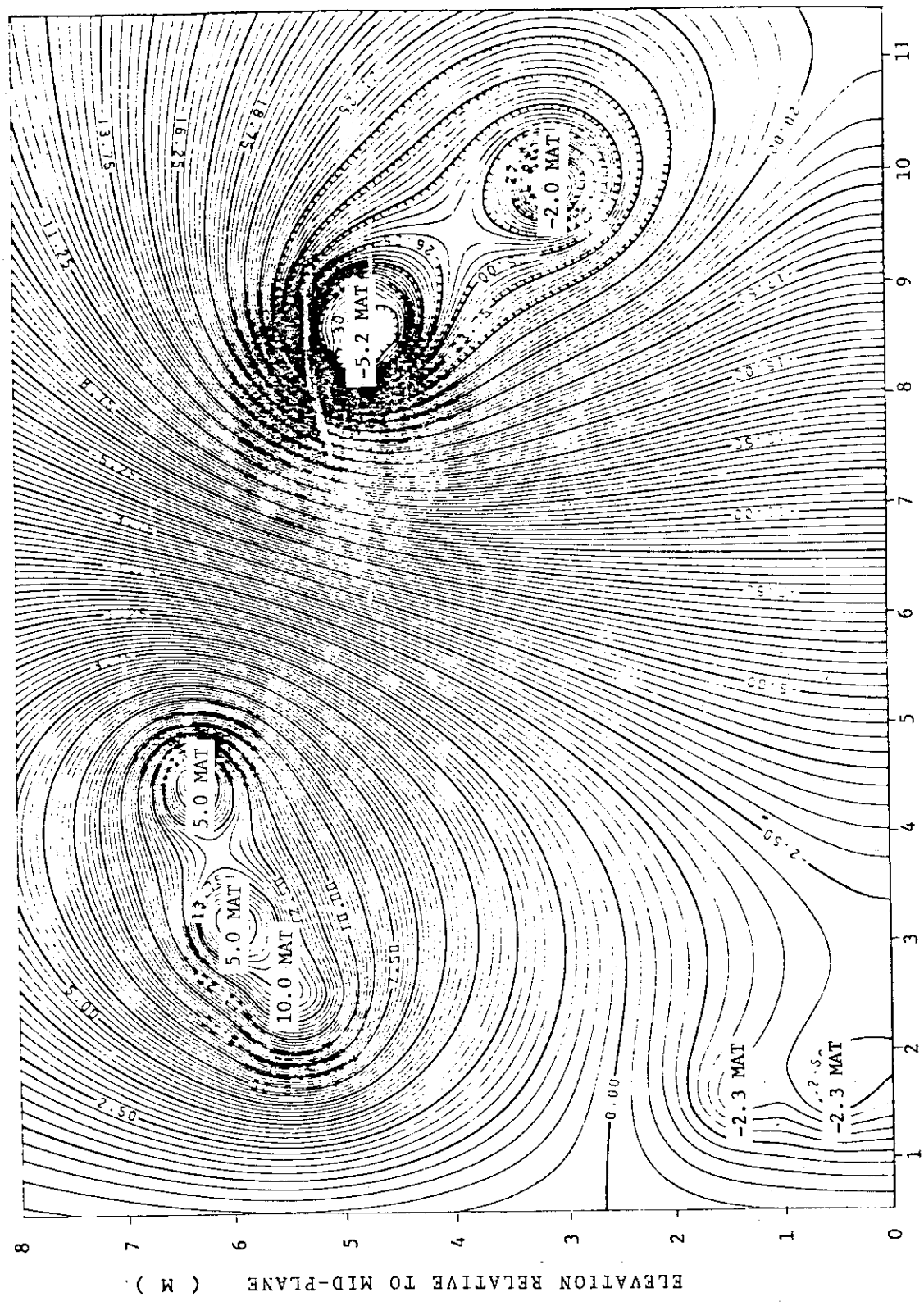

Fig. 4 Magnetic field configuration by external conductor, divertor configuration

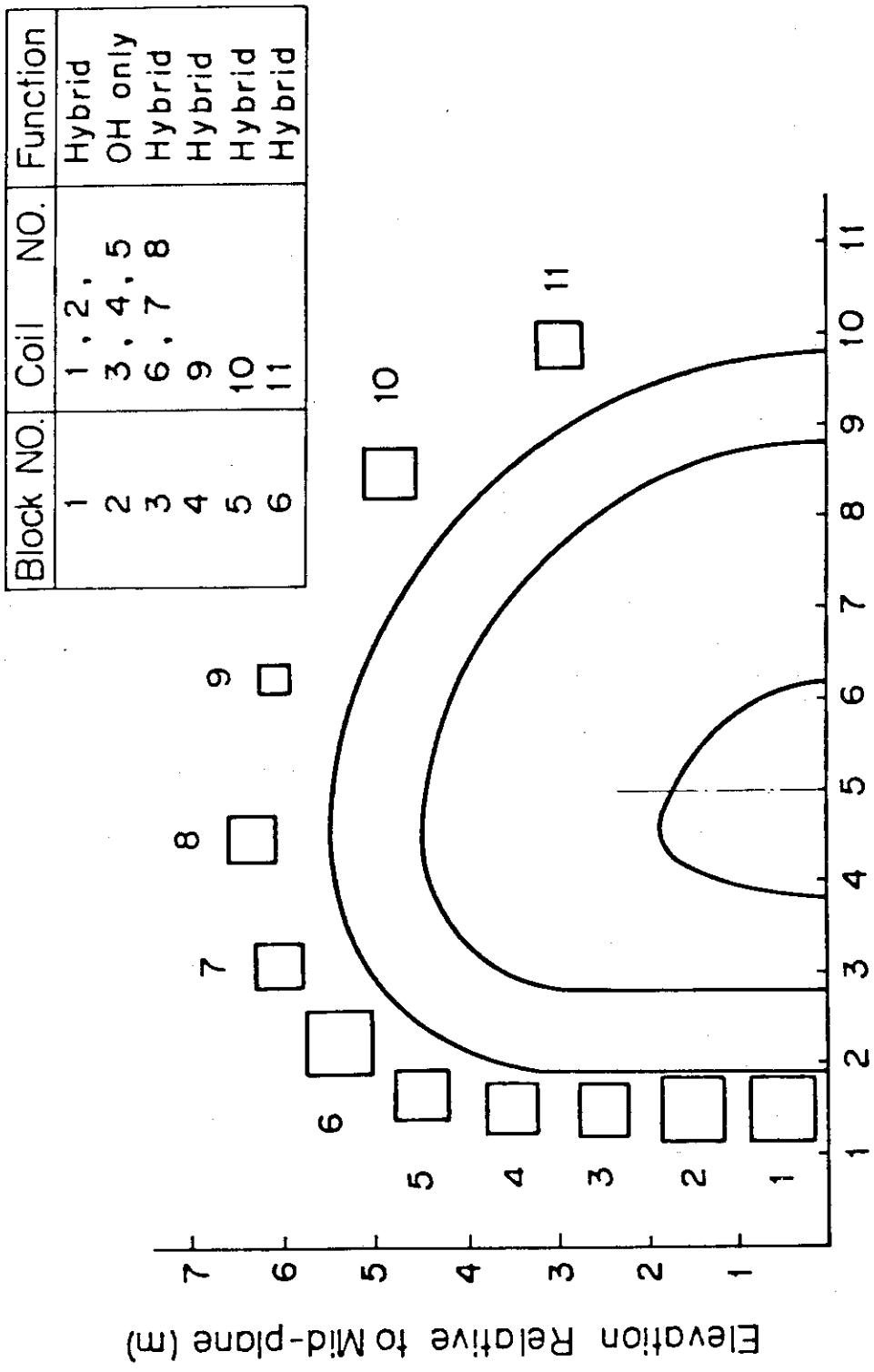

Fig. 5 INTOR Hybrid Poloidal Coil Locations

2.3 One-Dimensional Simulation of Ignition Approach

2.3.1 Calculation Model

Ignition approach has been investigated by one-dimensional transport code[1]. The transport coefficients used are

$$\chi_e = \frac{5 \times 10^{19}}{n_e} \frac{1}{\kappa} \quad (m^2/s) \tag{1}$$

$$\chi_i = 3 \times (\chi_i)_{neoclassical} \times \frac{1}{\kappa} + \chi_{ripple} \tag{2}$$

$$D = \chi_e / 12 .$$

Pellet injection was employed for tritium density build-up in joule heating phase. By this method, the plasma density is increased beforehand suitably for NBI heating. The plasma current rise time is 5 seconds. Neutral beam injection heating is started at t = 5 sec. We employ deuterium injection with 200 keV energy. NBI is turned off at t = 9 ∿ 10s. Particle recycling and fueling method will have a great influence on the attainability of the ignition through the density distribution. We employed puffing and pellet injection for the fueling method, and calculated for various recycling conditions. Both deuterium and tritium particles recycle with a given recycling rate, while helium particle recycling is not taken into account. Impurity effects are neglected in all of the calculations.

2.3.2 Results of simulations

A typical example of the ignition approach by gas puffing and recycling for the fueling method is shown in Fig. 1. The attainability of the ignition is very marginal. In fact, the ignition is achieved for 0.5 % toroidal field ripple, while the ignition fails to be achieved for 0.8 % ripple.

Time evolutions of various plasma parameters are shown in Fig. 2. Although $\bar{T}i$ is considerably high for 0.5 % field ripple, it can be lowered down to 12 ∿ 13 keV if suitable field ripple is applied or NBI heating time and power are suitably adjusted. Density profile is always very broad and slightly hollow. For this reason, the plasma is very sensitive to the field ripple, and moreover, higher beta value (> 4 %) is required to attain the ignition.

Time evolution of the various plasma parameters for pellet injection is shown in Fig. 3. We have assumed that the particle source profile by pellet injection is linearly decreasing one as shown in Fig.4[2]. Since the density profile is greatly affected by the penetration depth ℓ of the injected pellet. We have assumed that the injection velocity and the radius of the pellet are 10^4 m/s and 3 mm, respectively. These values seem to be the maximum expectable ones.

If the density profile is sharp even in large device, the ignition can be attained much easily even when the toroidal field ripple is larger. In fact, when we employ the flat particle source distribution (Fig. 6) the density and temperature profiles in nearly steady state become sharp. In this case, the ignition can be attained even for 1.5% ripple (Fig. 5). In Fig. 5, solid line of T_i shows the case where temperature rise is controlled by field ripple, so that the beta value does not exceed the critical value too much. In actual case NBI heating time and power and/or toroidal field ripple are adjusted to suppress the excessive rise of T_i. If no particular control is done, temperature rises up to 25 keV (dotted line of T_i shows the case of 0.5% field ripple).

Detailed discussion on the ignition scenario including transport models is given in the report of Group 1.

Results of 1D simulation calculations are summarized as follows.

The attainability of the ignition in INTOR is very sensitive to the physics model and operation scenario, especially to the density profile. Flat density distribution is most likely in INTOR even though strong inward particle flux such as Ware pinch effect is considered and realistic pellet injection is employed. In this case, ignition can be achieved in the guiding model only when toroidal field ripple is very small ($\lesssim 0.5\%$) and there is no impurity contamination.

Moreover, sufficient heating of central region by NBI of 200 keV injection energy is difficult and ripple loss of fast ions becomes serious for such flat density profile. Favourable dependence of χ_e on T_e as observed in PLT could make the achievement of ignition easier. Higher density ($\bar{n}_i > 1.4 \times 10^{20}$ m^{-3}) could also enable us to achieve ignition.

For sharp density profile, if realized, the ignition can be achieved rather easily in the guiding model when serious impurity contamination can be prevented.

References

1) T. Tone, K. Maki, et al. : in preparation for publication.

2) S.L. Milora, C.A. Foster, "ORNL Neutral Gas Shielding Model for Pellet-Plasma Interactions", ORNL/TM-5776, Oak Ridge National Laboratory, Oak Ridge, Tennessee (May 1977).
A.T. Mense, Q.A. Houlberg, S.E. Attenberger and S.L. Milora, "Effects of Fueling Profiles on Plasma Transport", ORNL/TM-6026, Oak Ridge National Laboratory, Oak Ridge, Tennessee (April 1978).

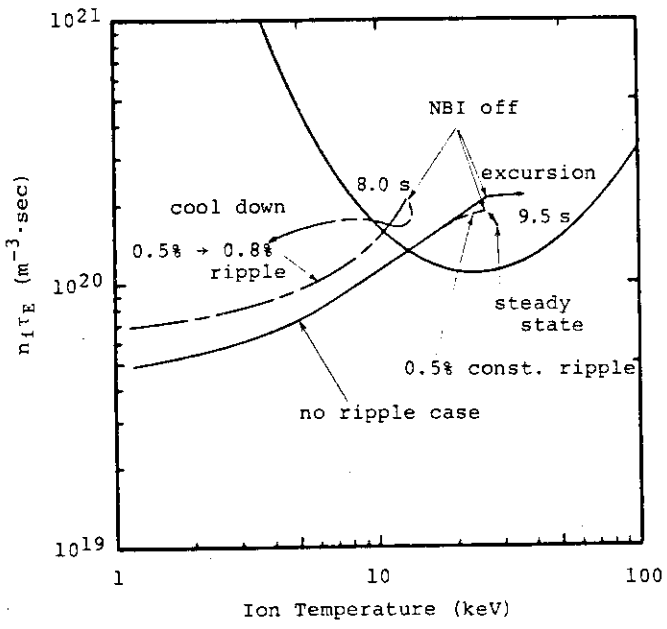

Fig. 1 Ignition approach by gas puffing for the fueling method. NBI heating power is 60 MW and is started at t=5.0s and stopped at t=9.5s in no ripple and 0.5% constant ripple case, and at t=8.0s in case of 0.5% → 0.8% ripple. 0.5% → 0.8% ripple means that the toroidal ripple is raised at t=7.5s from 0.5% to 0.8% with time constant of 2 sec.

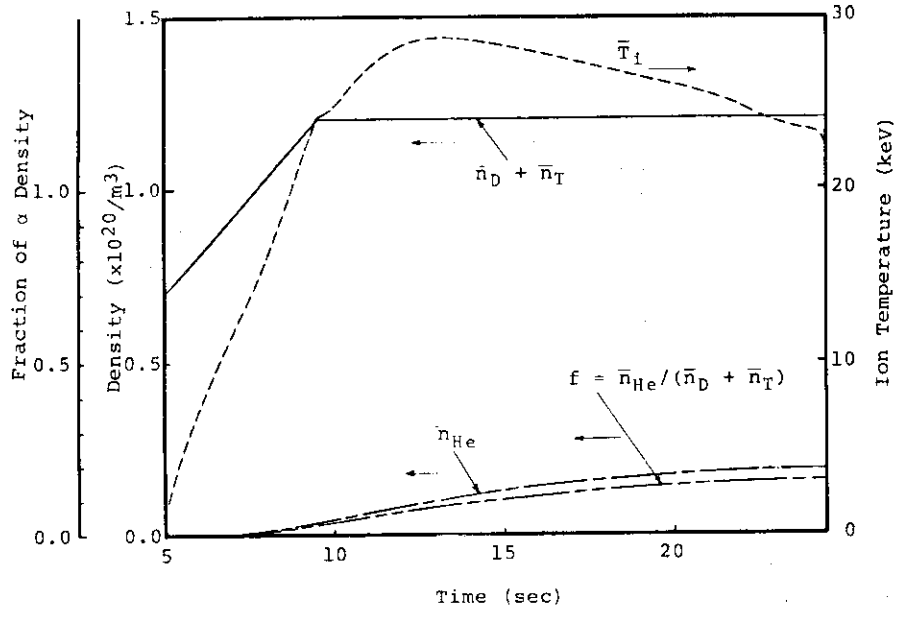

Fig. 2 Time evolutions of average fuel density ($\bar{n}_D+\bar{n}_T$), ion temperature $\bar{T}_i$, helium ash density $\bar{n}_{He}$ and fraction of ash f in gas puffing case. Toroidal field ripple is 0.5%. Because He ash accumulates and Bremsstrahlung increases, $\bar{T}_i$ gradually decreases after about 13 sec. $\bar{T}_i$ can be controlled at ∿15 keV by NBI heating time and power, and toroidal ripple.

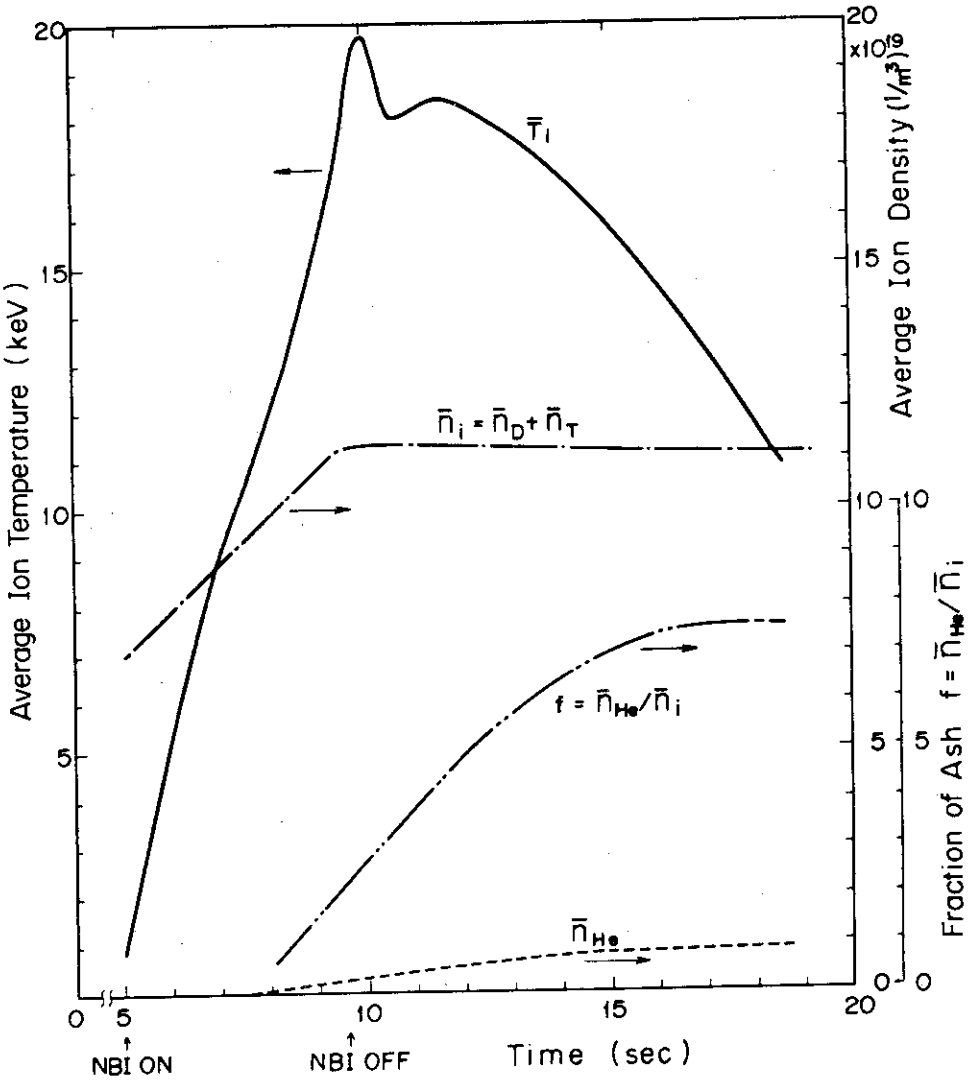

Fig. 3 Time evolutions of average ion density $\bar{n}_i$, ion temperature $\bar{T}_i$, helium ash $\bar{n}_{He}$ and fraction of ash f. Toroidal field ripple is 0.8%. Although $\bar{T}_i$ excessively rises up to 20 keV, this can be lowered (down to 12 ∿ 13 keV) by the control of NBI heating time and power or adjusting the toroidal field ripple (pellet injection case).

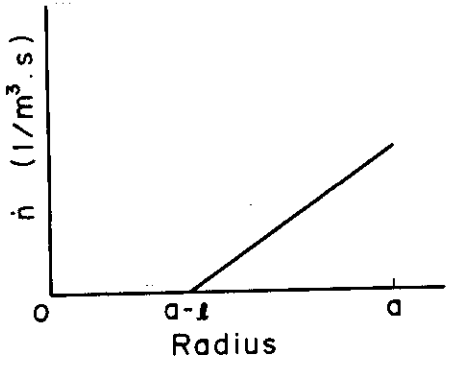

Fig. 4 Model of particle source profile by realistic pellet injection

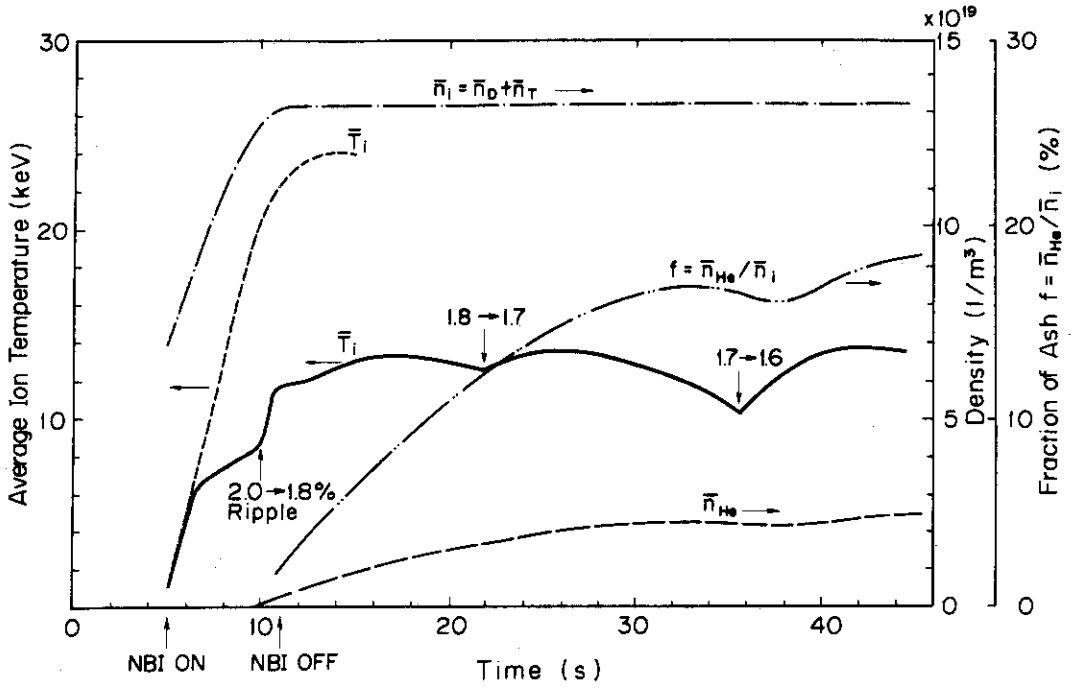

Fig. 5 Time evolutions of average ion density $\bar{n}_i$, ion temperature $\bar{T}_i$, helium ash $\bar{n}_{He}$ and fraction of ash f in the case of particle source profile shown in Fig. 6. The arrows on $\bar{T}_i$ curve show that toroidal field ripple is lowered to control the plasma temperature at that moment. The accumulation time (saturation time) of helium ash is about 20 seconds. When no particular control is done, $\bar{T}_i$ rised up to 25 keV (dotted line).

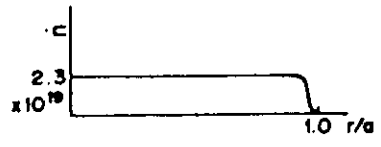

Fig. 6
Model of particle source profile by pellet injection. This source profile is employed to obtain a sharp density profile.

2.4 RF Heating Schemes for Start-up Phase

For RF heating schemes for the parameter range encountered during heating a plasma to an ignition state (2×10^{19} m^{-3} $\leq \bar{n}_e \leq 1.5 \times 10^{20}$m^{-3}, 1 keV $\leq \bar{T} \leq$ 10 keV), the following two schemes are considered for LHH as shown in Fig. 1.

The LHH systems provided are

A.	pump wave frequency	f = 1.2-1.4 GHz
	parallel refractive index	$N_{//}$ = 3 - 4
	deposit power	P = 10-20 MW
B.	pump wave frequency	f = 2.3 - 2.7 GHz
	parallel refractive index	$N_{//}$ = 2 - 3
	deposit power	P = 75 MW

The system A is operated for heating a plasma with $\bar{n}_e = 2 - 6 \times 10^{19}$m^{-3} and the system B is adopted when the plasma density increases beyond about 6×10^{19}m^{-3}.

The heating conditions mentioned above are reduced from the linear theory on the wave propagation and the power deposition. This is justified by the fact that the effective ion heating was achieved in JFT-2 when the turning point predicted by the linear theory located in the plasma, though non-linear effects were observed.

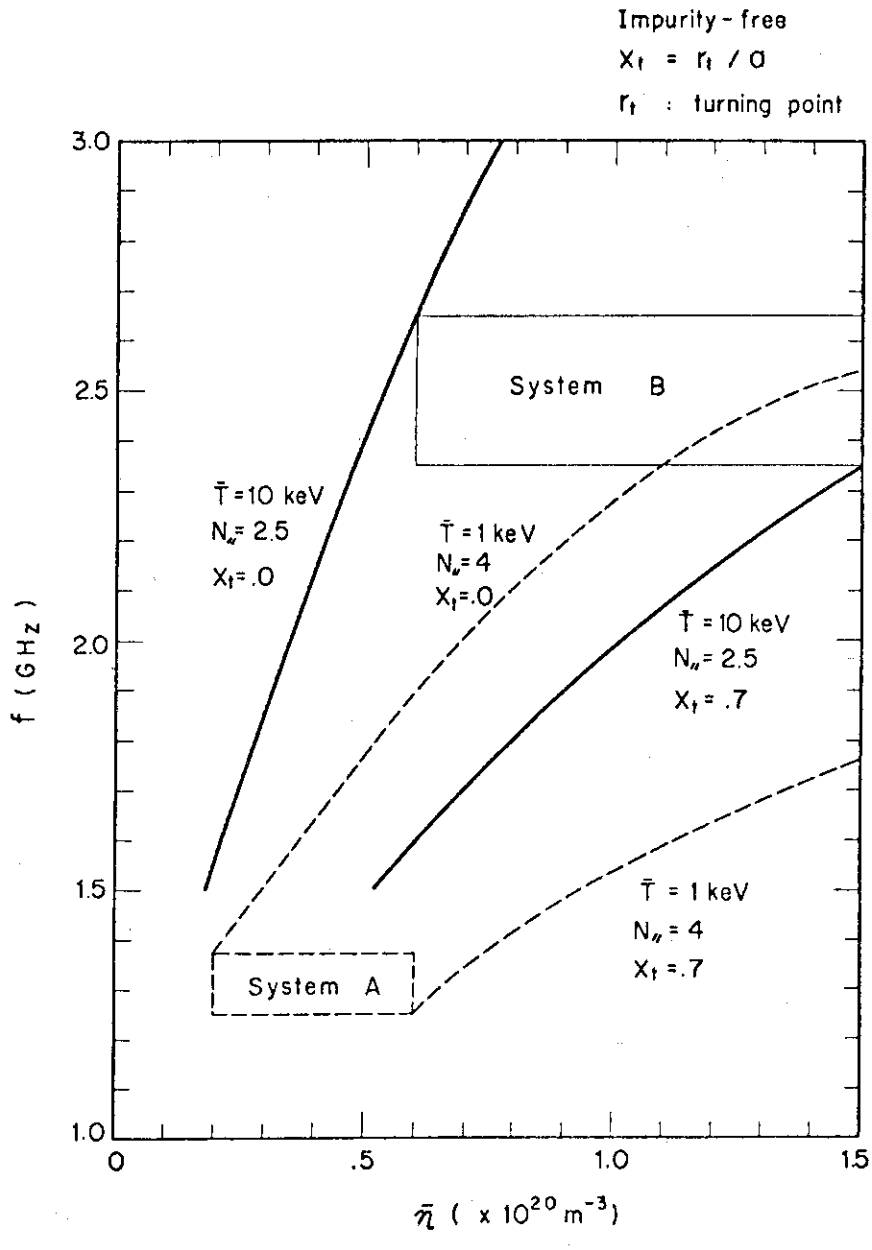

Fig. 1 Dependence of pump wave frequency on the plasma density. Dotted curves indicate the frequency adequate for the core heating ($0 \leq x_t \leq 0.7$, x_t : turning point normalized by a minor radius) in the case of $\bar{T}$ = 1keV and $N_{//}$= 4. Solid curves are obtained in the case of $\bar{T}$=10 keV and $N_{//}$=2.5. The accessibility condition is satisfied in each curve.

3. BURN

3.1 Limitation of Pulse Length due to Alpha-Particle Accumulation

If no successful exhaust means is available, the pulse length depends on a β-limit alone. With the INTOR parameters of $P_w^n \sim 1$ MW/m^2, $\bar{T}$ = 10 keV and $\bar{n} = 1.2 \times 10^{20}$ m^{-3} ($\beta_t \sim 4$ %), assuming parabolic profiles for temperature and density, a margin of 1 % (absolute value) in the β_t - value allows about 30 s burning time without the ash exhaust. n_α/n_i reaches 0.1 in 16 s and 0.2 in 32 s.

The following relation holds in the operation generating a constant power.

$$\frac{n_\alpha}{n_i} = \frac{1}{2} \frac{1}{\eta_D} \frac{\tau_\alpha}{\tau_f} \left(1 - e^{-\frac{\eta_D}{\tau_\alpha} t}\right) \qquad (1)$$

where τ_α is the confinement time of alpha particles, τ_f the time constant for fusion reactions and η_D the effective exhaust coefficient of alpha particles. If $\tau_\alpha \propto n a^2$,

$$\frac{\tau_\alpha}{\tau_f} \propto \beta^2 \frac{\langle \sigma v \rangle}{T^2} . \qquad (2)$$

The variation of $\langle \sigma v \rangle / T^2$ with plasma temperature is small in the range of 10 ∼ 20 keV, at most a 10 % change. Consequently, the pulse length is determined by obtainable η_D and allowable n_α/n_i.

For the INTOR parameters, τ_α/τ_f is about 2×10^{-2} ($\tau_\alpha \sim 1.5$ s, $\tau_f \sim 80$ s). The value of n_α/n_i reaches 0.2 in $24\tau_\alpha$ for η_D = 0.01 and in $28\tau_\alpha$ for η_D = 0.02. The values of η_D = 0.01 ∼ 0.02 would be available without a special physics scenario for ash exhaust. As mentioned above, the β-value increases by about 1 % in absolute value for these burning times which are about twice those without any ash exhaust.

When we want to obtain a longer pulse length, we have to consider physics scenarios for the solution of the ash exhaust which enhance η_D or decrease τ_α. If there is a margin of ∼ 1 % in β and $\eta_D \sim 0.05$ is realized, a long burn pulse would be possible. The enhancement of η_D would be possible by the ash enrichment near the exhaust ports. τ_α would decrease by enhancing the particle recycling at the plasma boundary. Ash enrichment and ash exhaust by simple poloidal divertors have been proposed[1], and a realistic and credible reactor design on the basis of

the physics scenario has been developed for INTOR.[2)3)] The scenarios for aiming at the complete solution of the ash exhaust are given in the report of Group 3.

References

1) Y. Shimomura, K. Sako, K. Shinya : "Some Considerations of Ash Enrichment and Ash Exhaust by a Simple Divertor", JAERI-M 8294 (1979).

2) K. Sako, T. Tone, Y. Seki, H. Iida, et al. : "Engineering Aspects of the JAERI Proposal for INTOR (I)", JAERI-M8503 (1979).

3) K. Sako, T. Tone, Y. Seki, H. Iida, et al. : "Engineering Aspects of the JAERI Proposal for INTOR (II), JAERI-M8518 (1979).

3.2 Current Control

Methods of external control of current profile are categorized typically into two groups : control of the electrical conductivity of a plasma and local drive of plasma current.

(1) Control of electrical conductivity

Local heating of electrons results in a change of the electrical conductivity of plasmas. Radio-frequency wave heatings such as ECRH and LHH are appropriate for this purpose.

The ECRH wave for INTOR requires a frequency near around 140 GHz, and hence the high power (several megawatts) generator technologies in such a high frequency range are essentially required. The LHH of electrons is performed with a pump wave having a large number of Nz (larger than about 10) and a frequency of a few GHz.

(2) Local drive of plasma current

The unidirectional parallel injection of a neutral beam can drive a plasma current locally. This scheme, however, is associated with design difficulties of Tokamak system as well as injector.

Another method of current drive can be provided by the Landau resonance of plasma electrons with injected pump waves.

The LHR wave is most preferable for the current drive from view points of the wave generator technologies and the position control of the driven current. From a simple analysis on the wave-particle interaction at the Landau resonance velocity, the current generation of several hundreds kA is sufficiently possible by launching a wave with $f \sim 3$GHz, $Nz \geq 10$ and 10MW RF power into the plasma.

3.3 Temperature Control

3.3.1 Burn stability (zero-dimensional calculation)

The critical temperature which defines a thermally stable region of plasma operating conditions is sensitive to the form of confinement time scaling. For self-ignition or subignition at high Q_F the Alcator and classical scalings yield high critical temperatures. The critical temperatures for self-ignition, namely, the minimum thermally stable temperatures are 27 and 39 keV, respectively, which are obtained from a global energy and particle balance model.

In Figs. 1 ∿ 3[1] are shown the critical temperature as a function of the parameters Q_F or $P_{inj}/(\beta_t B_t^2)^2$ (P_{inj}: MW/m^3, B_t: W_b/m^2) and stable regions in the $n\tau$ - T figure. With $Q_F \lesssim 5$, the critical temp-rature for all scaling laws decreases to half their $T_{c\infty}$ - values ($Q_F = \infty$). In order to operate at a temperature in the range of 10 ∿ 20 keV and within a β-limit, the means of controlling the burn stability is inevitably required. Controllability of a driven plasma with $Q_F \sim 5$ by fueling or heating was elucidated[2)3)] for the actual reactor design, JXFR[3)4)].

Two self-regulating mechanisms to suppress the growth of thermal instability have been assessed. One is the synchrotron radiation and the other is the field ripple diffusion. The effect of the former is small, even if the absorption coefficient of the wall is assumed to be unity. On the other hand, the latter markedly reduces the critical temperature.

The heat transport coefficient due to the ripple diffusion used for the analysis is simple represented as

$$\chi_i^r = 7.77 \times 10^{10} C \frac{T_i^{7/2}}{n_i} \delta_r^{9/2} \qquad (m^2/s) \qquad (1)$$

where T_i is the ion temperature (eV), n_i the ion density (m^{-3}) and δ_r the field ripple, respectively, and here C is set to 3.9×10^4 (see the report of Group 1). For simplicity the ripple diffusion was evaluated with an average ion temperature. The critical temperature in the global model depends on the temperature used for the evaluation of the ripple diffusion. The use of the average temperature might estimate the stable temperature at a low value. The evaluation of the ripple diffusion effect is made by a one-dimensional simulation code in the next section.

For example, the stable ion temperatures obtained from a zero-dimensional global model are 13, 19 and 26 keV for the field ripples

(δ_r) of 0.5, 0.4 and 0.3 %, respectively. If effects of the ripples on ion thermal conduction and NBI heating are not serious, a larger ripple could reduce stable operation temperatures down to near 10 keV.
If special coils generating a variable field ripple can be installed, deleterious effects of a large ripple during start-up phase is eluded.

If the ripple diffusion effect is not large enough to give a stable working temperature, some control means is necessary. Figures 4 and 5 exemplify the possibility of the burn control for sub-ignition at high Q_F ($\sim$30). In Fig. 4 the on-off control of heating power is applied to the plasma excursion initiated by -0.5 keV ion temperature perturbation at an equilibrium state of $Q_F \sim 30$. Such a control means would require a heuristic programming based on operation experiences.

In Fig. 5 the heating power proportional to the power perturbation initiated by 1.0 keV ion temperature perturbation is injected with a time delay of 0.5 s (Δt_d). The α_B indicates a proportional coefficient for the feedback control. In this case the ripple diffusion is not considered. The controllability for the case considering the ripple diffusion is similar to that in Fig. 5 except the initial few seconds where the variation of the parameters with time is more rapid because of the large effect of the ion temperature on the ripple diffusion.

In this model the feedback control is applied as detecting the power level at all times. As a result, it requires continuous heating whose total power during the burn duration would be about twice as much as that of the on-off control. The ion density is maintained at the initial value through fueling. Consequently the ultimate equilibrium values of the ion temperature and fusion power slightly exceed their initial values.

It would be desirable to exercise the feedback control within about 0.5 s for subignition at high Q_F ($\sim$30). The feedback control model used is classical. It would be preferable to use the multi-variable feedback control[5)]

For self-ignition the self-regulation mechanism such as the field ripple diffusion is essentially necessary, while for sub-ignition controlling the burn is possible without such an inherent control mechanism. If the operating temperature for self-ignition is in the unstable region, the burn control is possible by enhancing the field ripple in periodic pulses with use of some special coils to suppress the plasma excursion. For example, assuming the inherent field ripple of 0.5 % generated by TF coils, the burn is controlled by the feedback

enhancement of the ripple with a time delay of 0.25 s. The additional field ripple is about 0.1 % at its maximum. The absolute values of the ripple mentioned here are not essential, since the model used is a rough zero-dimensional one. Considering the required electric power and control system and the value of the additional field ripple, however, it would be preferable to generate the stationary field ripple required for stabilization.

References

1) T. Tone : J. Nucl. Sci. Technol., 16 [6], 453 (1979).
2) T. Tone, H. Yamato, K. Maki : Proc. 2nd Topical Meeting on the Technology of Controlled Nuclear Fusion, Richland, 1976, Vol. III, 975 (CONF-760935).
3) K. Sako, T. Tone, Y. Seki, H. Iida, et al. : "First Preliminary Design an Experimental Fusion Reactor", JAERI-M 7300 (in Japanese), (1977).
4) K. Sako, T. Tone, Y. Seki, H. Iida, et al. : Proc. 6th Conf. on Plasma Physics and Controlled Nuclear Fusion Research, Berchtesgaden, 1976, Vol. III., 239 (IAEA, Vienna, 1977).
5) Fusion Reactor System Laboratory : "Design Studies on Diagnostic Instrumentation and Control Systems for the JAERI Experimental Fusion Reactor", JAERI-M 8411 (in Japanese), (1979).

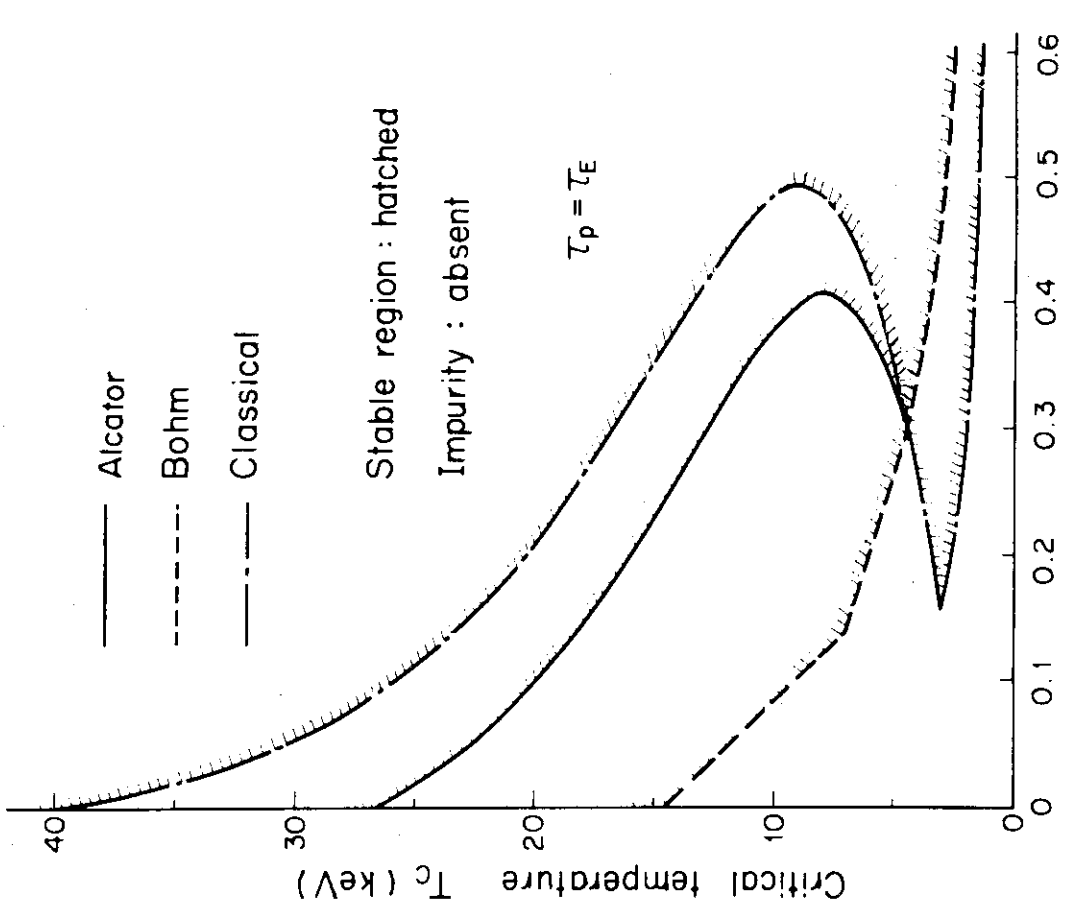

Fig. 2 Critical temperature as a function of injection power. P_{inj} : MW/m^3, B_t : W_b/m^2

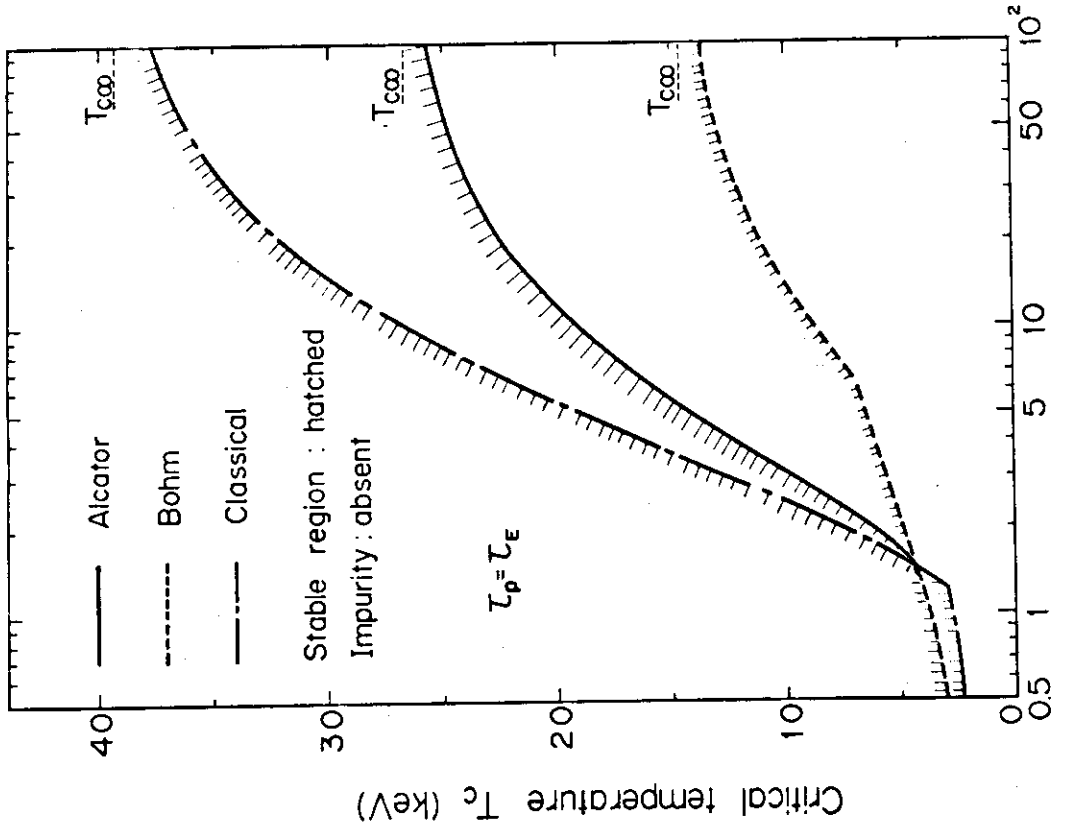

Fig. 1 Critical temperature as a function of Q_F

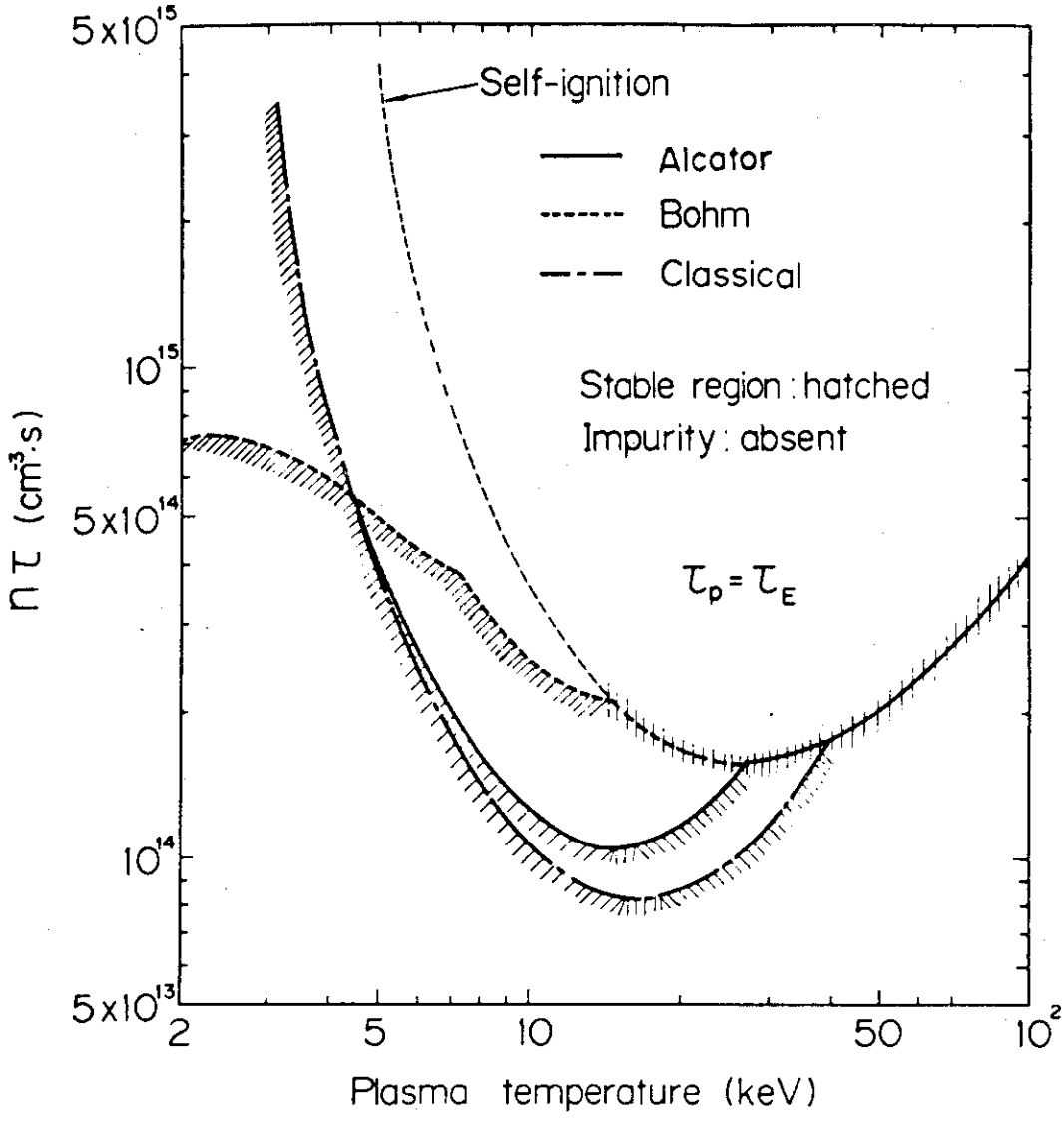

Fig. 3 Stable regions in the nτ-temperature figure

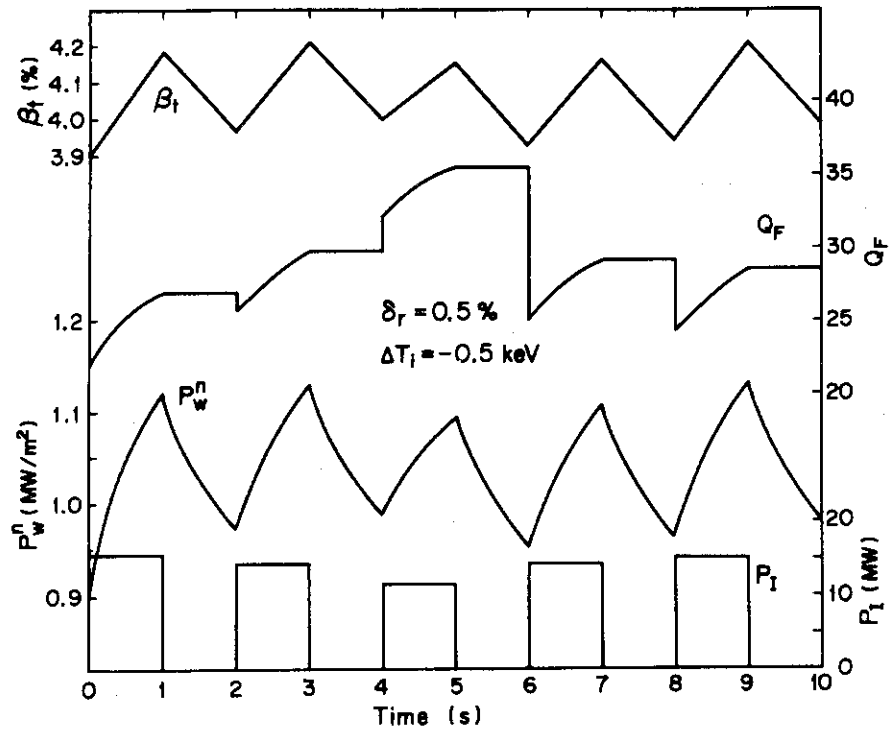

Fig. 4 An example of the on-off control of heating power for stabilizing the plasma excursion initiated by -0.5keV ion temperature perturbation at an equilibrium state of $Q_F \sim 30$

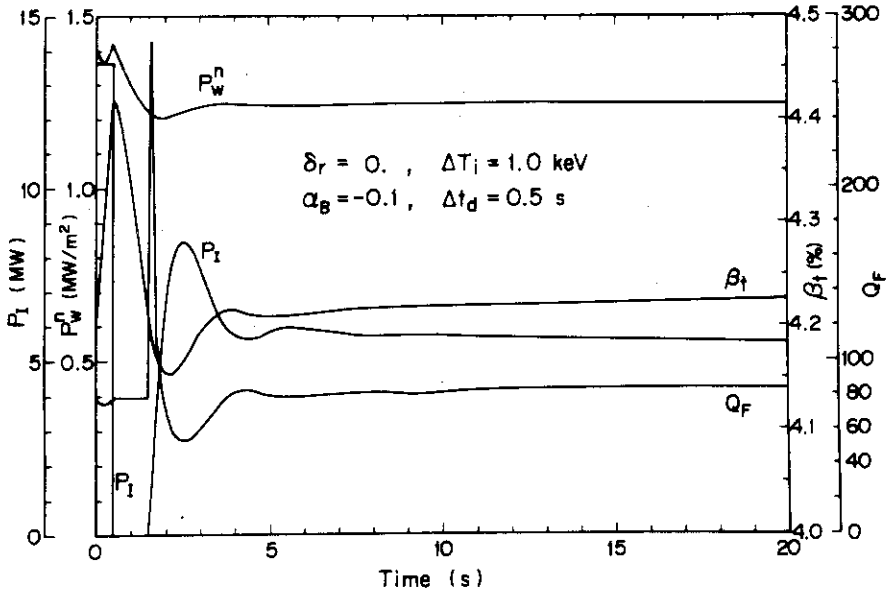

Fig. 5 An example of the feedback control by heating power for stabilizing the plasma excursion initiated by 1.0keV ion temperature perturbation at an equilibrium state of $Q_F \sim 30$. Delay time for feedback control: 0.5S.

3.3.2 Burn control by a variable field ripple (one-dimensional calculation)

A toroidal ripple will suppress the temperature excursion. However, the ripple value during neutral beam injection should be kept low. When the self-ignition state are attained, the ripple must be raised immediately from the base value to the desired one. If the rise time of the variable ripple is long, the plasma temperature will overshoot and β value will exceed its critical value.

We have evaluated the required ripple value and its rise time necessary for suppressing the temperature excursion by one-dimensional simulation code[1], and estimated the electric capacity of the variable ripple coil power supply. The toroidal ripple δ is expressed by the following equations in our simulation code.

$$\delta = \delta_a(t) \cdot (r/a)^2 \tag{1}$$

$$\delta_a(t) = \begin{cases} \delta_o & t < t_o \\ \delta_o + \delta_v\{1 - \exp(-\frac{t-t_o}{\tau})\} & t \geq t_o \end{cases} \tag{2}$$

where, $\delta_a(t)$; ripple value at plasma surface,
δ_o ; base ripple value,
δ_v ; variable ripple value,
t_o ; start time of the variable ripple,
τ ; time constant for raising ripple.

Fig. 1 shows the simulation results of the start up and burn phase. Gas puffing is used for fueling. In the case of no ripple, the plasma temperature does not make an excursion unlike no ripple case, and stays at about 15 keV in the case of 0.7 % ripple. This temperature is a stable point. In this case, we can operate the reactor without feedback control of burning. However, the plasma temperature and β value will inevitably be higher than those of INTOR guiding parameters as shown schematically in Fig. 2. If there is no margin in β value, the size of plasma or toroidal field should be increased for obtaining thermally stable plasma. As shown by curves c and d in Fig. 1, the control of neutral beam injecting time or power is very effective to suppress the temperature overshoot. This situation is schematically illustrated in Fig. 2. The temperature at the end of the start-up phase, T_3, should be between T_1 (unstable point) and T_2 (steady state point) in order to reach the stable point with minimizing the overshoot. The plasma temperature

rises from T_3 to T_2 with time constant of several seconds. Furthermore, there would arise no serious problem, even if the ripple begins to be raised a little before neutral beam stops. Therefore, if the variable ripple is raised with time constant of a few seconds, the overshoot would be no matter.

The magnetic energy of the variable ripple field is about 10^{-4} times as small as that of the toroidal field, i.e. a few MJ. Then, the required electric power will be order of 1 MW, assuming the rise time of a few seconds. Even if 10 MW is required, the power would not be so significant.

Reference

1) T. Tone, K. Maki, et al. : in preparation for publication.

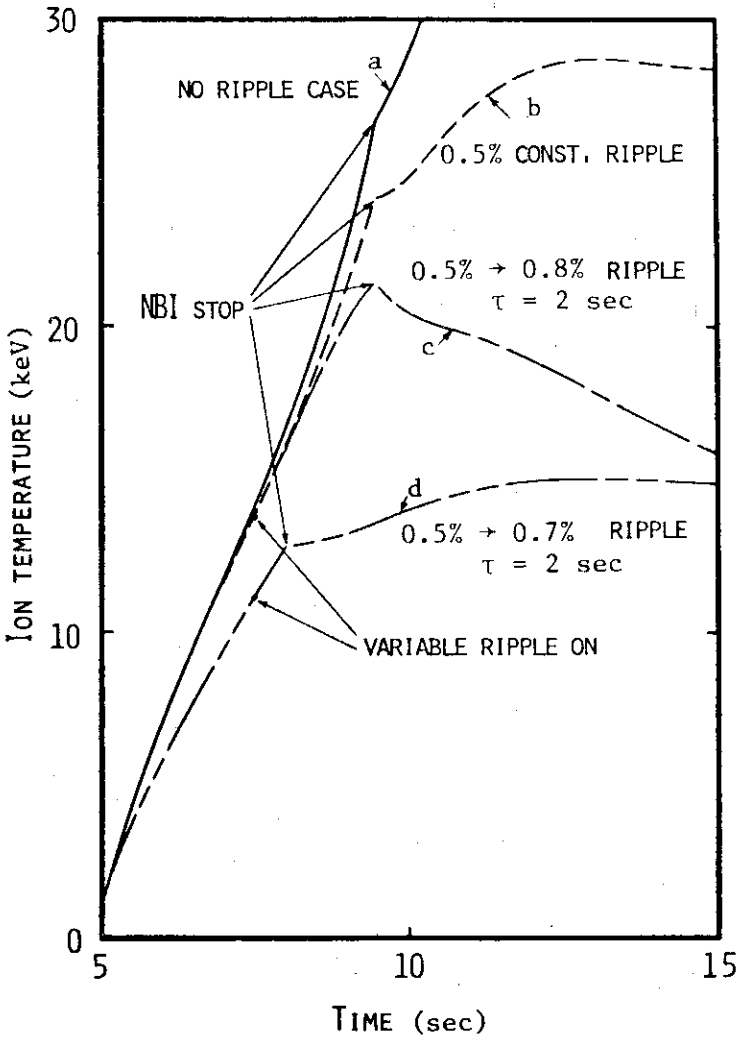

Fig. 1 Ion temperature time evolutions of start-up phase in case of ripple control. Curve a is for no ripple case, curve b is for 0.5% base ripple case. In case of c and d, the variable ripple is raised at t = 7.5 sec from 0.5% base value to 0.8% and 0.7% respectively with time constant of 2 sec.

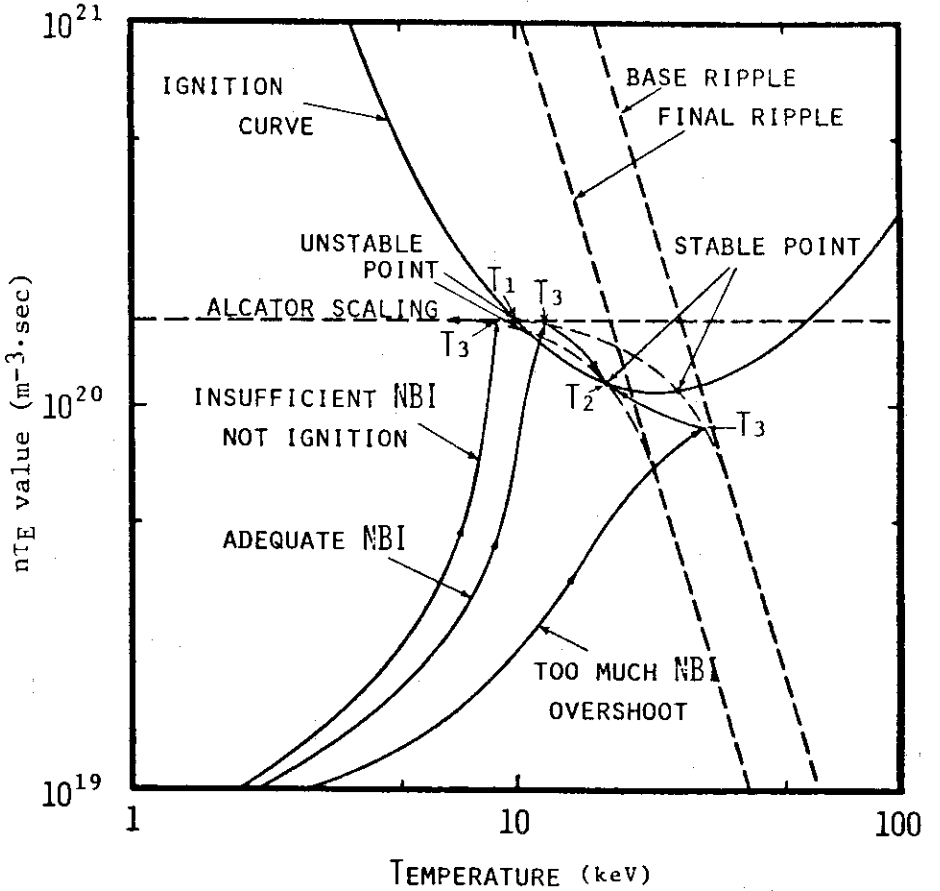

Fig. 2 Schematic feature of the start-up phase. In case of insufficient NBI, the temperature decreases after NBI stops. In case of too much NBI, the temperature overshoots. In adequate NBI case, the temperature increases to the stable point without overshoot.

3.3.3 Control of temperature profile

(1) Neutral beam injection

By choosing appropriate beam energies, the power deposition profile of the beam can be changed. This method provides the most simple method of the temperature profile control.

(2) Wave heating

(a) ECRH

By choosing appropriate frequencies in a range of 100 $\sim$ 140 GHz, the ECRH makes it possible to control the temperature profile of the plasma.

The essencial difficulty lies in the high power (an order of MW) wave generator technologies in the necessary frequency range.

(b) LHRH

By changing the number of Nz, the LHRH can be used for controlling the power absorption region in space.

(3) Surface cooling by low-Z impurities

Injection of low-Z materials can provide a means of controlling the plasma surface temperature.

(4) Current profile control

By changing the radial position of the magnetic resonance surface through the current profile control, the temperature profile can be deformed appropriately. The formation of an ergodic region around the resonance surface can enhance the temperature profile deformation.

3.4 Reactor Relevant Burn Pulse

In this section we estimate the minimum burn time required to attain net electric power production, i.e. the time at which $Q^* = \bar{P}_{el,total}/\bar{P}_{el,into\ reactor}$ becomes larger than unity. The bar above the symbol means time average.

Conditions provided for the calculation are the followings.

(1) Hybrid poloidal field coils.

(2) NBI is used for additional heating.

(3) Only neutron energy contributes to electric power production.

(4) Energy recovery from poloidal field coils is taken into consideration.

(5) Direct energy conversion from divertors is omitted.

(6) Appropriate energy dissipation in the Helium liquifier and refrigerator and the power consumption in the auxiliary system e.g. He coolant blower are introduced. These energy dissipations are assumed to be time-independent.

The power load pattern of the poloidal field coils is showen in Fig. 1, and the meanings of the symbols are explained in Table 1.

During premagnetization of the OH coils, coil currents are increased up to the level to be interrupted for initiating gas breakdown and plasma current rise. Linear increase of the coil currents are assumed so that the energy dissipation during the premagnetization becomes

$$\int_0^{T_I} R_{OH} \left(\frac{t}{T_I} \right)^2 dt = \frac{1}{3} R_{OH} T_I .$$

All inductive energy stored in the poloidal field coils E_{OH} during premagnetization is both transfered to the plasma and dissipated in the coils until the coil currents become zero. This energy can not be recovered electrically.

After the coil currents become zero they increase in the opposite direction continiously and the energy is supplied into the coils again. The situation is the same to the premagnetization, and then the energy dissipation during this opposite current rise is estamated at $\frac{1}{3} R_{HY} T_R$.

During flat top of the plasma current, coil currents must increase in order to maintain the plasma current, even if the change is very

small. The effect is expressed in the form of $E_{HY}\alpha T_B$. In large Tokamaks with high plasma temperature, α is much smaller than unity.

1) Net electric power production

On the bases described above, we have the next equation for the net electric power production,

$$\eta P_n T_B \geq E_{OH} + E_{HY}(1+\alpha T_B)(1-f) + R_{OH}T_I/3 + R_{HY}(T_R/3+T_H+T_B) + P_{inj}T_H/\eta_{inj} + P_{drv}T_B/\eta_{inj} + P_{ref}T_B/f_d + P_{aux}T_B/f_d \quad . \quad (1)$$

By using the normalization summarized in Table 1, the above equation is deduced to the following two equations.

$$T_B \geq \frac{\tau_{OH}+(1-f)\tau_{hy}+k_{OH}T_I/3+k_{HY}(T_R/3+T_H)+k_{inj}T_H/\eta_{inj}}{\eta-\alpha(1-f)\tau_{HY}-k_{HY}-k_{drv}/\eta_{inj}-k_{aux}/f_d} \quad (2)$$

$$\eta > \alpha(1-f)\tau_{HY}-k_{HY}-k_{drv}/\eta_{inj}-k_{aux}/f_d \quad (3)$$

2) INTOR parameters

To evaluate the net electric power production, we use the following designed parameters of INTOR.

P_n=350 MW, E_{OH}=670 MJ, E_{HY}=2380 MJ, R_{OH}=200 MW, R_{HY}=440 MW,
P_{inj}=50 MW, P_{drv}=15 MW, $T_I=T_R=T_H$=5 sec, η_{inj}=0.3, α=0.002.

$P_{ref}+P_{aux}$ is assumed to be 50 MW or 100 MW.

3) The case of normal conducting poloidal field coils

We have $k_{HY} > 1$, hence equation (3) is not satisfied, i.e. INTOR can not produce net electric power.

4) The case of super conducting poloidal field coils

We have $k_{OH} = k_{HY} = 0$. Results are shown in Figs. 2 - 6 in both cases of self-ignition and beam driven reactors. Assessment of the different type of reactors and the different span of burn times for the net electrical production is summarized in Table 2.

5) Conclusion

Beam-driven reactors can produce net electric power only in the long burnings at least in INTOR size. Short burning reactors require high electric conversion efficiency and duty factor, and the energy stored in the poloidal field coils should be effectively recovered. 100 MW $P_{ref}+P_{aux}$ seems to be the upper limit for the net electric power production even in the long burning reactors.

These situations are fairly improved if the α-particle energy can also be available for electric production, the amount of which is estimated at about 30 per cent or more of the neutron energy.

Table 1 Characters Used in the Calculation

Character	Quantity	Unit	Normalization
T_B	Burn Time	sec	
T_R	Plasma Current Rise Time	sec	
T_H	Additiona Heating Time	sec	
T_I	Premagnetization Time of Poloidal Field Coils	sec	
E_{OH}	Premagnetization Energy of Poloidal Field Coils	MJ	$\tau_{OH} = E_{OH}/P_n$
E_{HY}	Energy Stored in Poloidal Field Coils after the plasma current build-up	MJ	$\tau_{HY} = E_{HY}/P_n$
R_{OH}	Joule Loss during PFC Premagnetization	MW	$k_{OH} = R_{OH}/P_n$
R_{HY}	Joule Loss during Tokamak Discharge	MW	$k_{HY} = R_{HY}/P_n$
P_n	Neutron Output Power	MW	
P_{inj}	Injection Power for Additional Heating	MW	$k_{inj} = P_{inj}/P_n$
P_{drv}	Beam-Driving Power	MW	$k_{drv} = P_{drv}/P_n$
P_{ref}	Helium Refrigeration Power	MW	
P_{aux}	Auxiliary Power	MW	$k_{aux} = P_{aux}/P_n + P_{ref}/P_n$
η	Electric Conversion Efficiency		
f	Energy Recovery Efficiency of PFC		
η_{inj}	Overall Efficiency of Neutral Beam Injector		
f_d	Duty Factor of Operation		

Table 2 Possible Region of Net Electric Production

Time Scale	Self-ignition Reactor		Beam-driven Reactor	
	Super conducting PFC	Normal PFC	Super conducting PFC	Normal PFC
Short Burn ($\lesssim$ 60 sec)	possible only if $\frac{P_{ref} + P_{aux}}{P_n} \lesssim 0.15$, $\eta \cdot f_d \gtrsim 0.25$ and $f \gtrsim 0.5$	impossible	impossible	impossible
Long Burn (> 60 sec)	possible if $\frac{P_{ref} + P_{aux}}{P_n} \lesssim 0.3$ and $\eta \cdot f_d \gtrsim 0.15$	impossible	possible only if $\frac{P_{ref} + P_{aux}}{P_n} \lesssim 0.15$ and $\eta \cdot f_d \gtrsim 0.25$	impossible

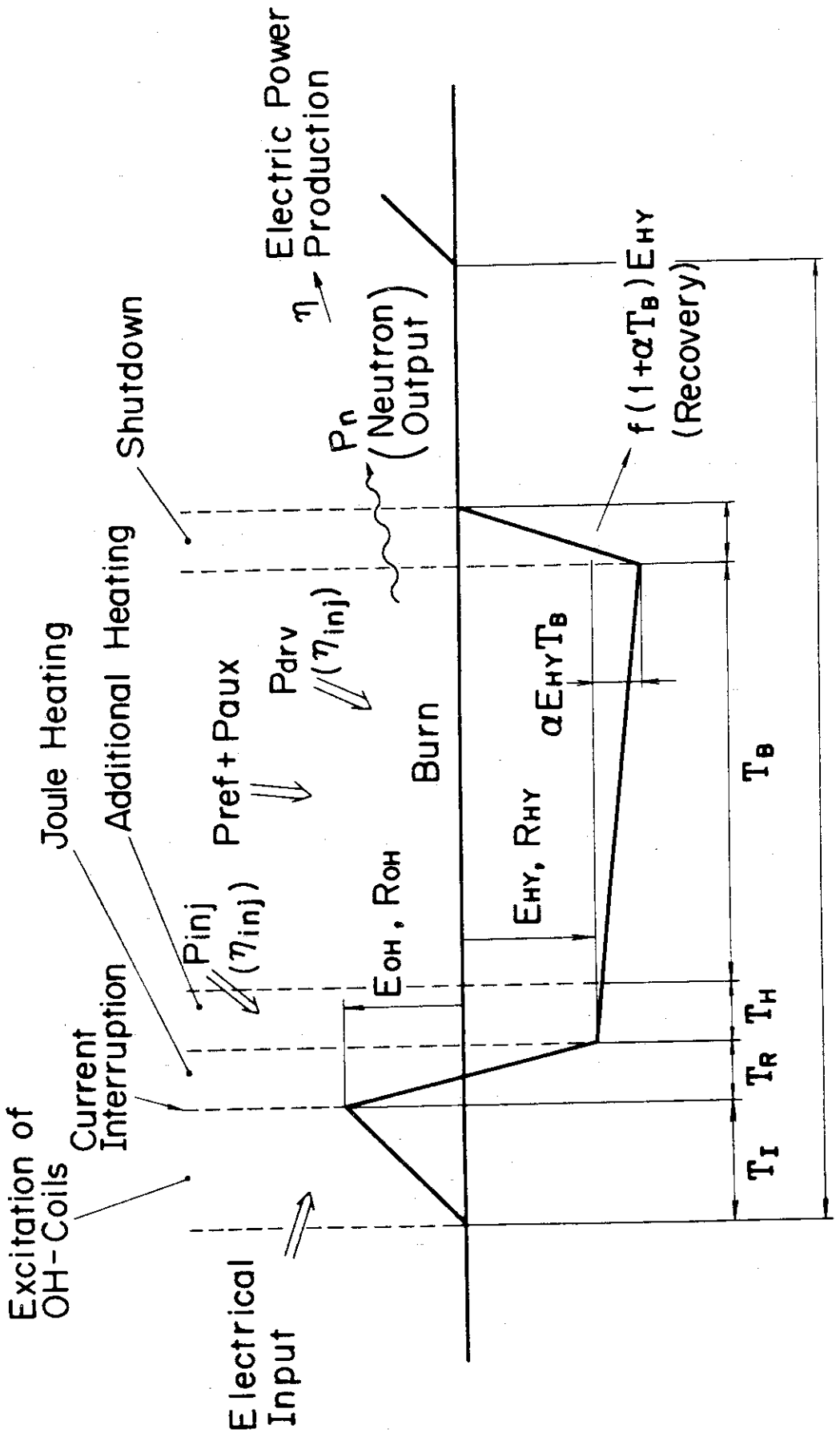

Fig. 1 Power load pattern of poloidal field coils

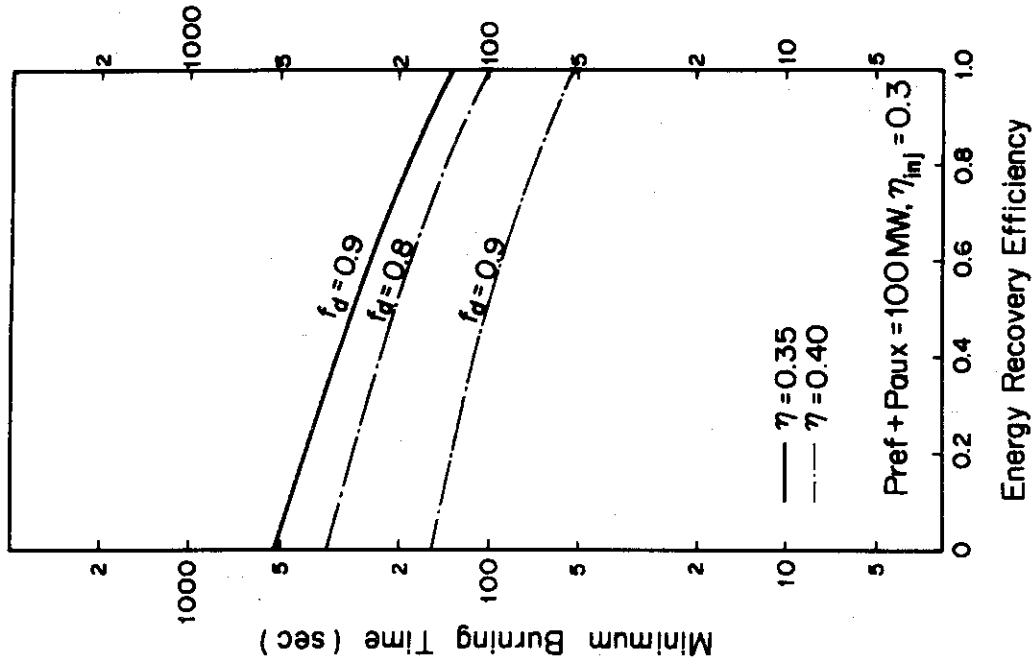

Fig. 3 Minimum burning time necessary for a self-ignition reactor to produce net electric power

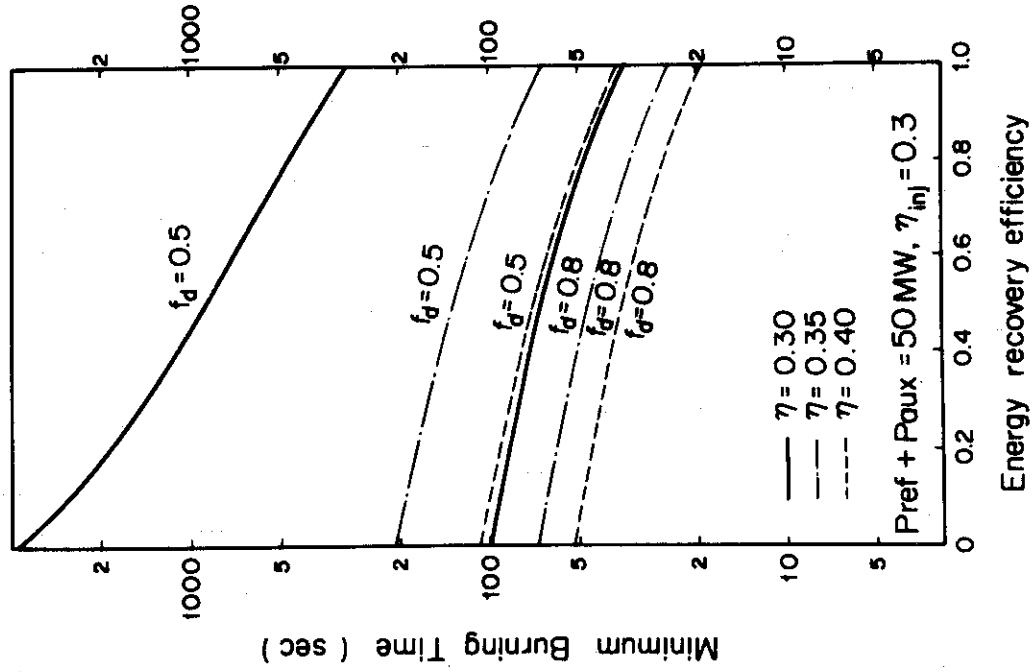

Fig. 2 Minimum burning time necessary for a self-ignition reactor to produce net electric power

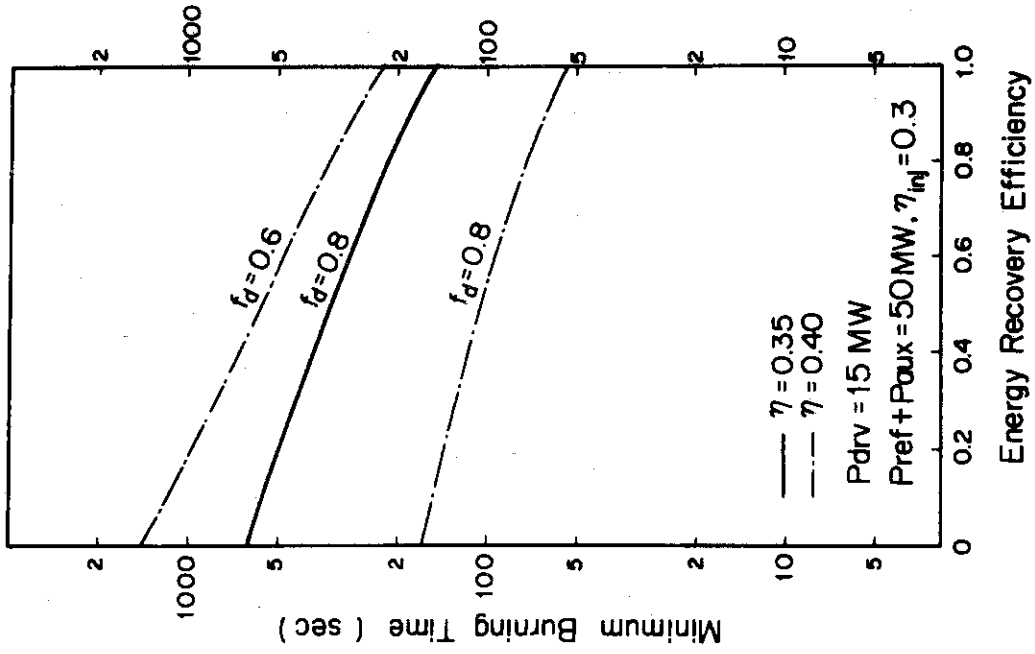

Fig. 5 Minimum burning time necessary for a beam-driven reactor to produce net electric power

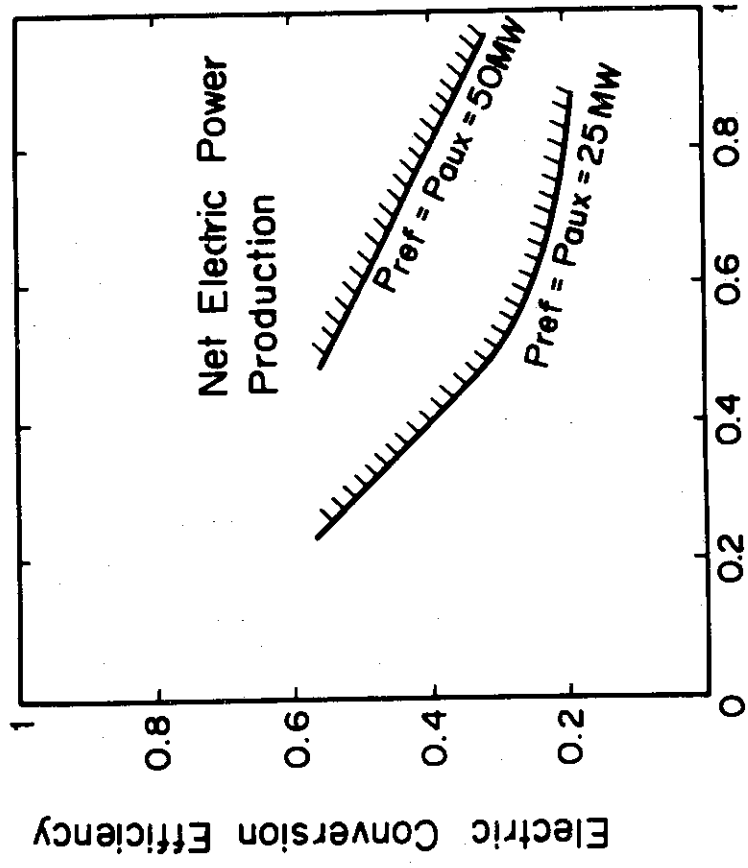

Fig. 4 Domain of net electric production for a self-ignition reactor

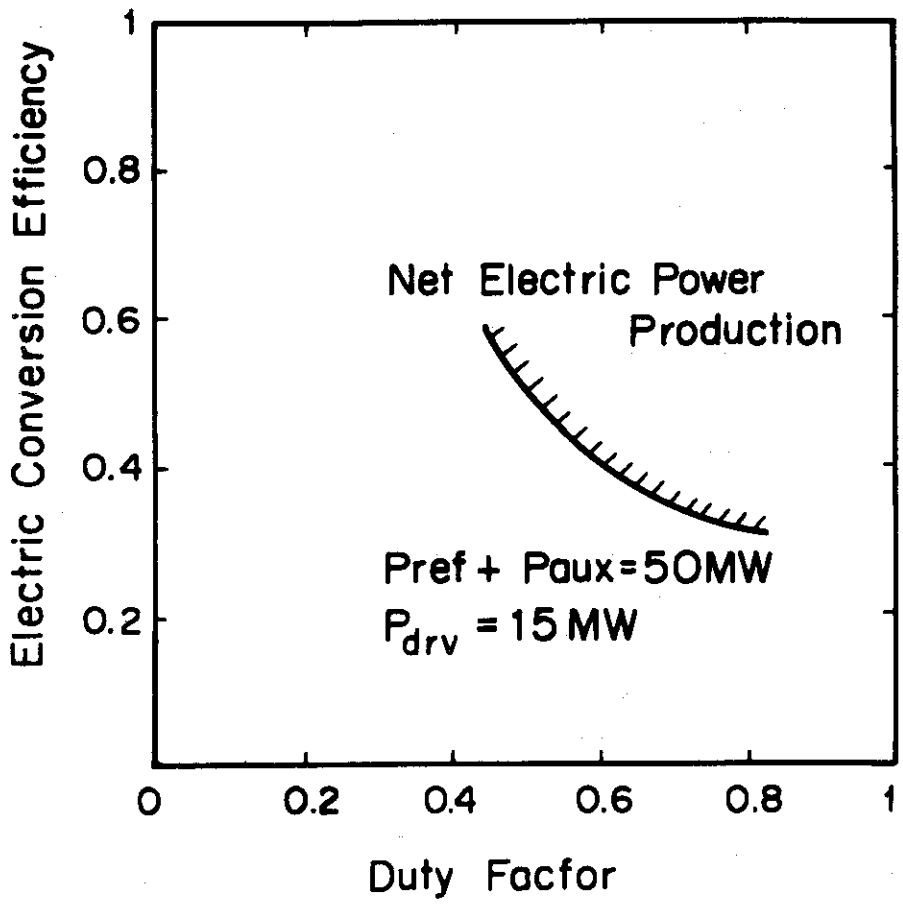

Fig. 6 Domain of net electric power production for a beam-driven reactor

3.5 Plasma Inductance and Flux Swing

The plasma inductance has been calculated by the ring model which was developed to determine the transient current on the vacuum vessel of JT-60. The inductance calculation has been made in axisymmetric toroidal plasma configurations. The plasma is divided into many conducting rings with a square-shaped cross section which are connected electrically through their mutual inductance. The current distribution of the INTOR plasma is expressed by 30 × 21 conducting rings.

The equation used for the inductance is

$$L = \frac{\sum_{\ell,m=1,n} M_{\ell m} J_\ell J_m}{\left(\sum_{\ell=1,n} J_\ell\right)^2}$$

where

$M_{\ell m}$: mutual inductance between rings ℓ and m ($M_{\ell\ell}$ is the self-inductance of ring ℓ)

J_ℓ : current of ring ℓ

n : total number of rings.

The radial current distributions at various z-coordinates are shown in Fig. 1. The inductance obtained for the current distribution is 12.9 μH. The flux swing (volt-second) required to raise and sustain the plasma current during the start-up and burning phases is given by

$$\Phi = L_p I_p + \int R_p I_p \, dt$$

The simulation calculation of the resistivity term is described in the report of Group 8.

The volt-second required for start-up (6s) is 67 v-s and the total volt-second for startup (6s) and flat-top (200s) is 88 v-s.

Note:

The build-up wave form of plasma current has been slightly modified as shown in Fig. 2; the build-up rater of the current is somewhat slowed down after t = 3.6 sec and the flat-top is reached at t = 6.0 sec (in the previous design, t = 5.0 sec). This modification was made to eliminate an extra peak in required power in the current build-up phase. For comparison the current rise scheme employed for a Session 2 task is shown in Fig. 3.

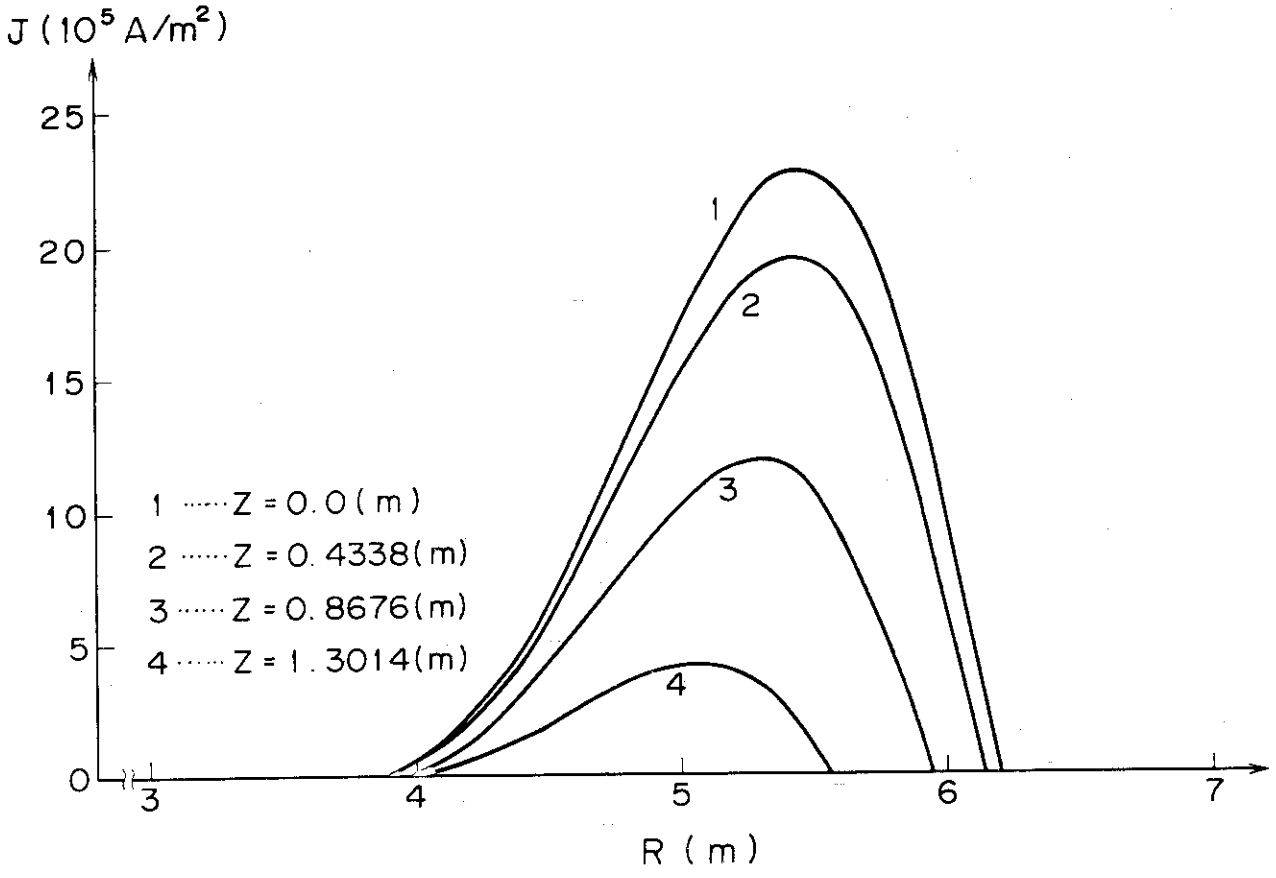

Fig. 1 Current distribution in INTOR plasma

Modified scheme of plasma current in the build-up phase

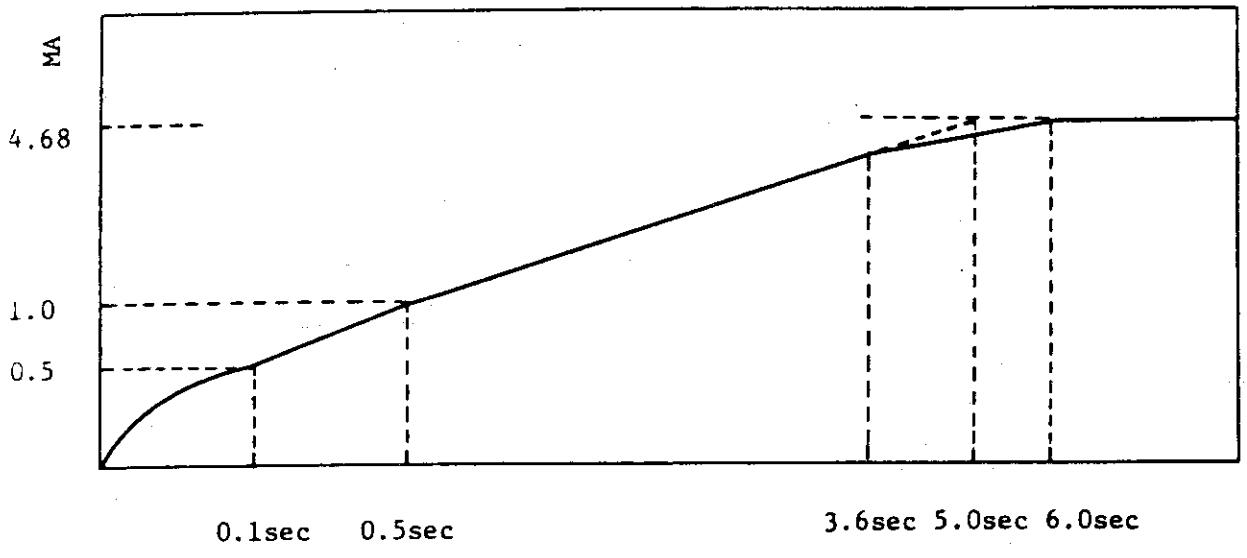

Fig. 2 Plasma current in the build-up phase (Session 3)

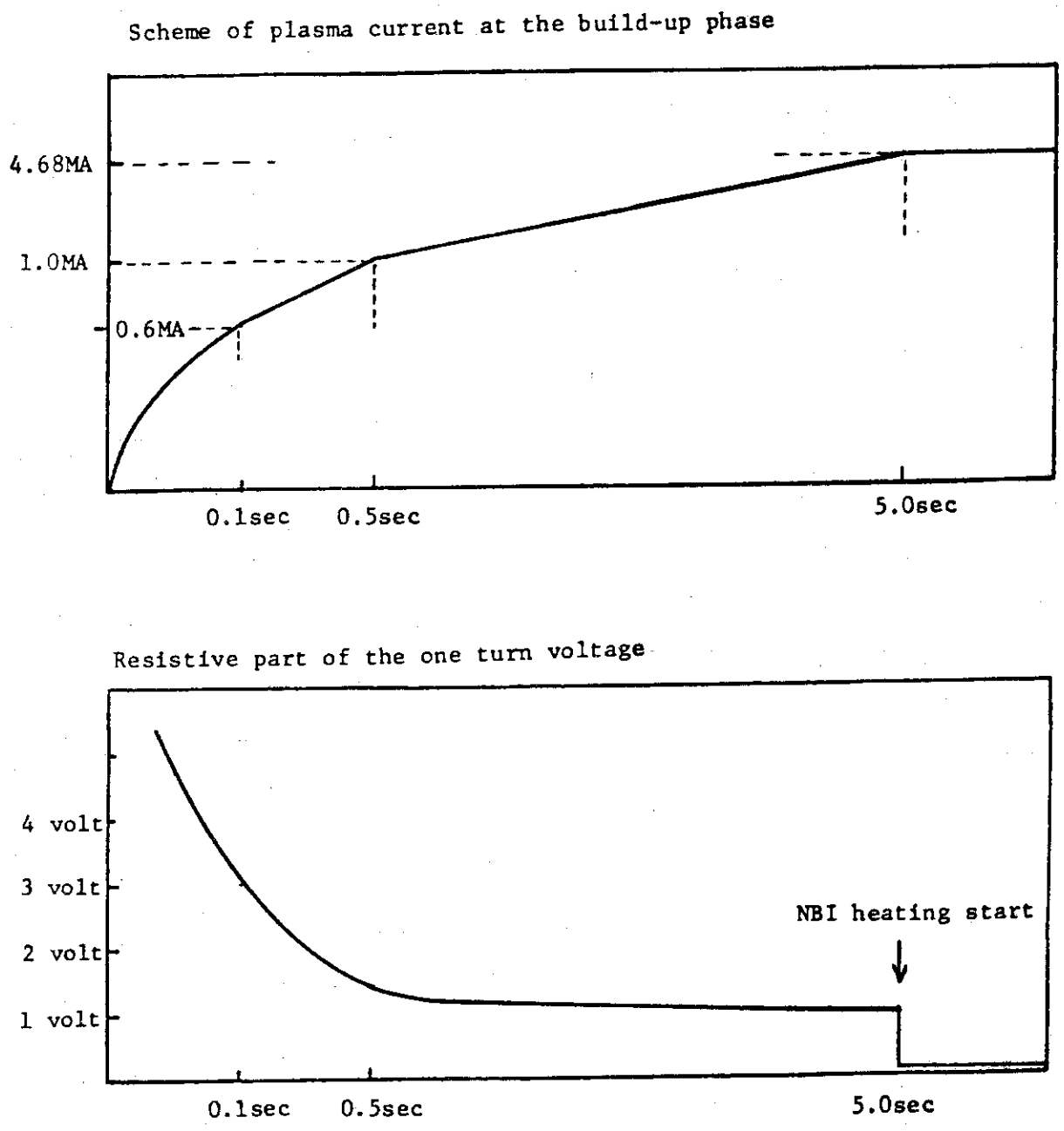

Fig. 3 Plasma current and resistive loop voltage in the current build-up phase (Session 2)

4. SHUTDOWN

For the self-ignition plasma the plasma is gently cooled to the state of $Q_F \sim 30$ if the fuelling is turned off. Fig. 1 shows the time dependence of the plasma parameters after the sate of $Q_F \sim 30$. In the case of the field ripple present the decrease with time is slow. The means of turning off the fuelling takes a relatively long time. If we want to cool the plasma in a short time, the addition of a small quantity of impurities would be effective.

In the case of using impurities attentions should be paid to avoid the occurence of disruptions. For use of heavy metal impurities there is a fear that the plasma center might be seriously cooled into disruption. As an impurity used for shutdown an inert gas such as Ne would be favorable.

For the driven plasma at low Q_F (~ 5) the plasma is immediately cooled by switching off the heating power but a rapid cooling which brings about the plasma quench should be avoided by controlling the decrease rate of the heating power.

It seems that there are no special difficulties in technologies for recovering the poloidal magnetic field energy. At the end of each pulse, the poloidal field energy is recovered to the generators to re-accelerate them for the subsequent operation. In the reference design calculation, the rotation of the generators almost reaches the maximum available rotation at the end of this phase (see the report of Group 8).[1)]

Reference

1) JAERI-M 8511, (1979)

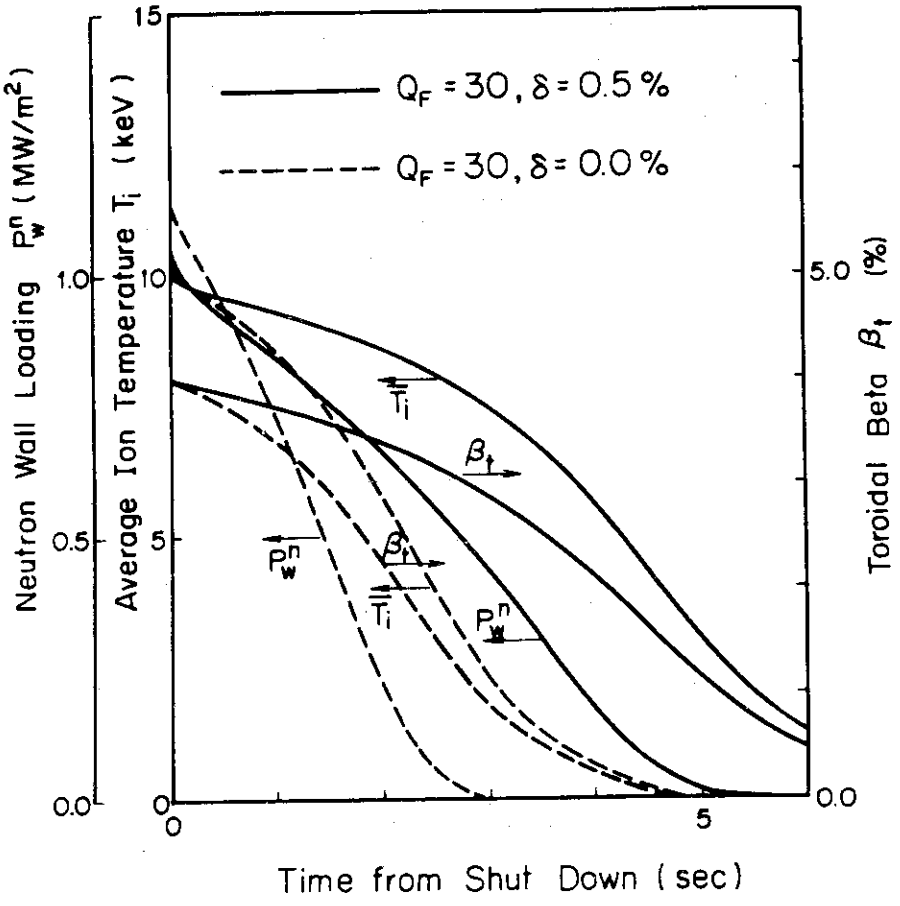

Fig. 1 Time evolution of the parameters in the shutdown phase

Appendix A

Model and Results of Gas Breakdown and Current Initiation

(presented at Session 2)

1) Model

The gas breakdown scenario for the INTOR has been made considering the increase of electron density and current, the variation of the magnetic error field which impedes the increase of the electron density, and the electric field over the plasma column cross section. The discharge evolution process was analysed with the parameters $P_0 \simeq 10^{-4}$ Torr and initial voltage < 100 V, for which runaway electrons do not play an important part. Under these conditions the ionization processes are fairly accurately described by the conventional equations.

We have modified them by adding some equations for the electric field time variation which penetrates inside the vacuum vessel by the rapid exitation of the OH power supply and for the variation of the error field in the vacuum vessel. It would be desirable to simplify the equations describing the breakdown mechanism. Here, a zero-dimensional model is used for the breakdown simulation.

We assume that the discharge chamber is initially filled with neutral atomic hydrogens of uniform density (N_0). The initial electron density is given by ξN_0, where ξ is the degree of ionization. The variation of the electron density is described by

$$\frac{dn_e}{dt} = \nu_i n_e - \frac{n_e}{\tau_e} \tag{1}$$

The ionization frequency is given by

$$\nu_i/p = 10^{-1.406(X-2.6)^2+8.946} \tag{2}$$

where $X = \log_{10}(E/p)$ and E/p is volt/cm·Torr.

The following equations is used for determining the diffusion time constant of electrons, τ_e:

$$\begin{aligned} \tau_e &= A/v_D \\ v_D &= v_e \times \frac{B}{B_T} \\ v_e &= 1.27 \times 10^6 \ (E/p) \quad (cm/sec) \end{aligned} \tag{3}$$

where v_e is the electron drift velocity which is related to the E/p, and A the vacuum vessel radius and B the magnetic field perpendicular to the toroidal magnetic field.

The time variation of B is described by

$$\frac{d}{dt} B + \frac{B}{\tau_V} = \frac{B_F}{\tau_V} \tag{4}$$

$$B_F = \frac{\mu_0}{4\pi R} (\ln 8R/A - 1.5) \times \frac{\text{One-turn voltage}}{R_V}$$

$$\tau_V = \frac{L_V}{R_V}$$

where R_V is the one-turn resistance of the vacuum vessel. B in Fig. A.1 is determined by the current redistribution on the vacuum vessel. The electric circuit of the INTOR OH power supply is modified as shown in Fig. A.2.

The other equations used are:

$$R_p = \frac{2R}{A^2} \eta \qquad \text{(plasma loop resistance)}$$

$$= \frac{1}{n_e \mu_{0e}}, \qquad \mu_0 = 1.27 \times 10^6 E/p$$

$$j = \frac{I_p}{\pi A^2} \qquad E = \eta j$$

$$M_{fV}\dot{I}_f + L_V\dot{I}_V + M_{Vp}\dot{I}_p + R_V I_V = 0$$

$$M_{fp}\dot{I}_f + M_{Vp}\dot{I}_V + L_p\dot{I}_p + R_p I_p = 0$$

2) Solutions of the equations

The model described above was applied to the parameters of JFT-2.[1] (see Appendix B). For the INTOR, the following parameters are used.

Initial neutral gas pressure	$p_0 = 10^{-4}$ Torr
Vessel one-turn resistance	$R_V = 0.2$ mΩ
One-turn voltage	50 V
Initial error field	180 Gauss
Initial degree of ionization	$\xi_0 = 2 \times 10^{-9}$
Toroidal field	$B_T = 50$ kG
Plasma radius	a = 1.5m, modified for a = 1.2 and b = 1.8

The time evolution of the total vessel current and the plasma current are shown in Fig. A.3(a). Figure A.3(b) preesent the time evolution of the loop voltage on the vessel and the resistive voltage of the plasma. Figure A.3(c) shows the voltage variation of the block No. 2 OH coil (240 turns) to which the voltage 10 kV is applied. Fig. A.4 shows the electron density evolution. The initial density is 7×10^3 /cm^3 which corresponds to $\xi_0 = 2 \times 10^{-9}$. At 30 mS, the electron density increases to 10^{11} /cm^3 which corresponds to the ionization degree of $\xi = 0.071$.

We could not apply the model further to the time phase after this time point, because it seems that the applicability of the model would be limited within the degree of ionization below 0.1. For the further time phase the ordinary tokamak transport simulation code should be applied.

Reference

1) T. Sometani and N. Fujisawa : Plasma Physics 20 (1978) 1101.

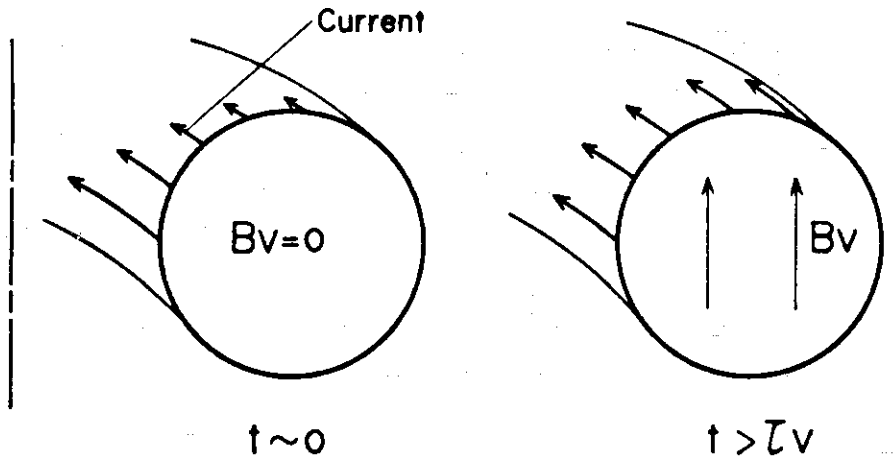

Fig. A.1 The vertical field generated by the redistribution of the loop current on the vacuum vessel.

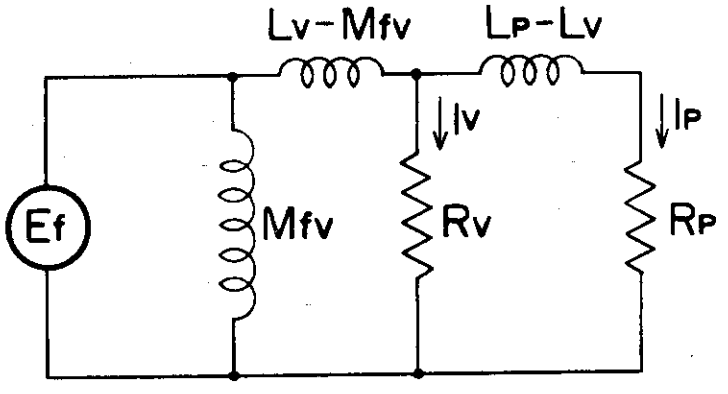

Fig. A.2 Schematic electric circuit of OH coil, vacuum vessel and plasma.

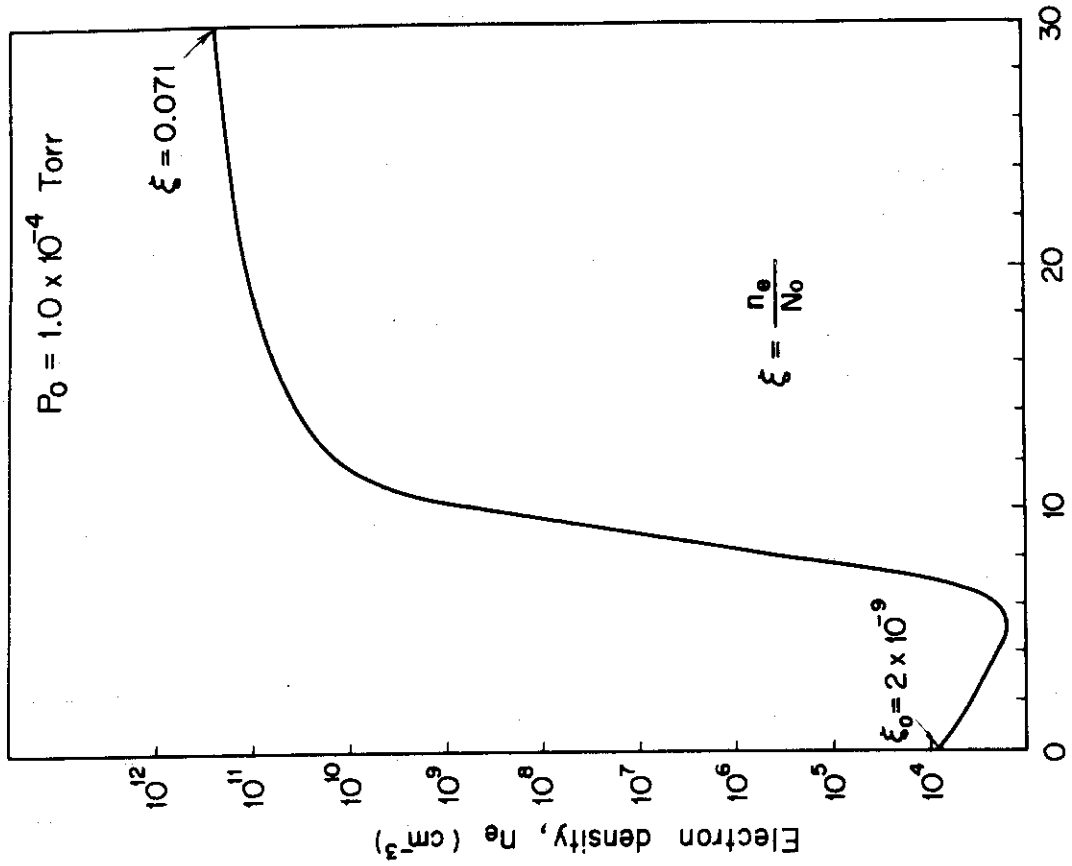

Fig. A.4 Time evolution of the electron density

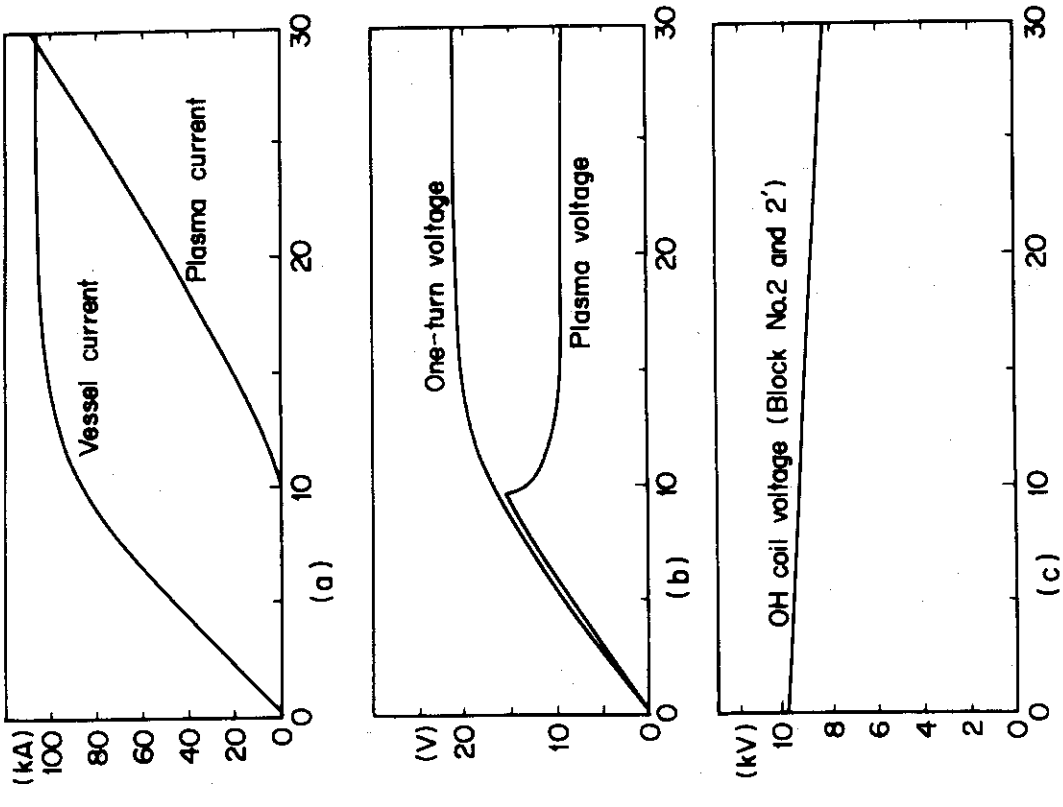

Fig. A.3 (a) Time evolution of the plasma current and vessel current, (b) the one-turn voltage of plasma, and (c) the OH coil voltage

Appendix B

Breakdown Simulation on JFT-2

Computer simulations on the breakdown process in JFT-2 tokamak were carried out with the model described in the preceeding report subjected to the Session 2. The effect of the -on-axisymmetric magnetic field is assumed to be 0.1% of the toroidal field.

The experimental results are shown in Figs. B.1, B.2 and B.3. Fig. B.4 shows the waveform of the oneturn loop voltage and Fig. B.5 is the well known zebra pattern of the associate electron density[1]. The conditions of the experiment and the simulation are listed in Table B.1. The initial degree of ionization is determined after the simulation to the value which might be the best fit to the experimental results.

The comparison of the simulation with the experimental results is shown in Fig. B.6 and Fig. 7. Fig. B.7 shows that the breakdown process is very sensitive to the error magnetic field. From these results, the model describes fairly well the experimental results.

The ionization frequency ν_I and the drift velocity V_E are calculated hydrogen atoms and molecules with maxwellian distribution.[2]

$$\frac{d}{dt} n_e = \alpha_{IN} N_N n_e + \alpha_{IM} N_M n_e \tag{B-1}$$

$$\frac{d}{dt} n_N = 2(\alpha_{DM1} + \alpha_{DM2}) n_M n_e + \alpha_{Da} n_a n_e - \alpha_{IN} n_N n_e \tag{B-2}$$

$$\frac{d}{dt} n_a = \alpha_{IN} n_M n_e - \alpha_{Da} n_a n_e$$

$$n_M = \frac{1}{2} (n_f - n_N - n_a - n_e) \tag{B-3}$$

α_I : ionization rate

$\alpha_{IN} : H^0 + e \rightarrow H^+ + 2e$

$\alpha_{IM} : H_2 + e \rightarrow H_2^+ + 2e$

α_D : dissociation rate

$\alpha_{CM1} : H_2 + e \rightarrow H^0 + H^0 + e$

$\alpha_{DM2} : H_2 + e \rightarrow H^0 + H^* + e$

$\alpha_{Da} : H_2^+ + e \rightarrow H^0 + H^+ + e$

α_{ex} : excitation rate $\quad \alpha_{ex} : H^0 + e \rightarrow H^* + e$

n_e : electron density, n_N : H^0 density, n_a : H_2^+ density,

n_M : H_2 density, n_f : all H density

$$\frac{d}{dt}\bar{v}_e = -\frac{e}{m}E - \nu_{eff}\bar{v}_e \tag{B-4}$$

$$\frac{d}{dt}n_e W_e = j E - n_e(\nu_I w_I + \nu_{DM1} w_{D1} + \nu_{DM2} w_{D2} + \nu_{ex} w_{ex}) \tag{B-5}$$

$$j = -e n_e \bar{v}_e \tag{B-6}$$

$$E = E_{ext} \tag{B-7}$$

$$\nu_{eff} = \nu_{eN} + \nu_{eM} + \nu_{ei} + (1 + \frac{1}{2}\frac{w_I}{W_e})\nu_I + \frac{1}{2}\frac{w_{D1}}{W_e}\nu_{D1} + \frac{1}{2}\frac{w_{D2}}{W_e}\nu_{D2} + \frac{1}{2}\frac{w_{ex}}{W_e}\nu_{ex} \tag{B-8}$$

$\nu_I \equiv \alpha_{IM} N_N + \alpha_{IN} n_M$, $\nu_{DM1} \equiv \alpha_{DM1} n_M$, $\nu_{DM2} \equiv \alpha_{DM2} n_M$,

$\nu_{ex} \equiv \alpha_{ex} n_N$,

$w_I = 13.6$ eV, $w_{D1} = 8.8$ eV, $w_{D2} = 14$ eV, $w_{ex} = 10$ eV

ν_{eN} , ν_{eM} , ν_{ei} : elastic collision frequency

The cross-section data of elastic and inelastic collision between electrons and hydrogen atoms and molecules are shown in Fig. B.8. From eqs. (B-1) to B-8), we obtain the relation of the electron drift velocity to electron temperature, and the dependence of the ionization frequency on the E/n_f. Figs. B.9 and B.10 show these relationship.

References

1) T. Sometani and F. Fujisawa ; Plasma Phys. 20 (1978) 1101

2) T. Takizuka ; Hohden Kenkyu 69 (1977) 31

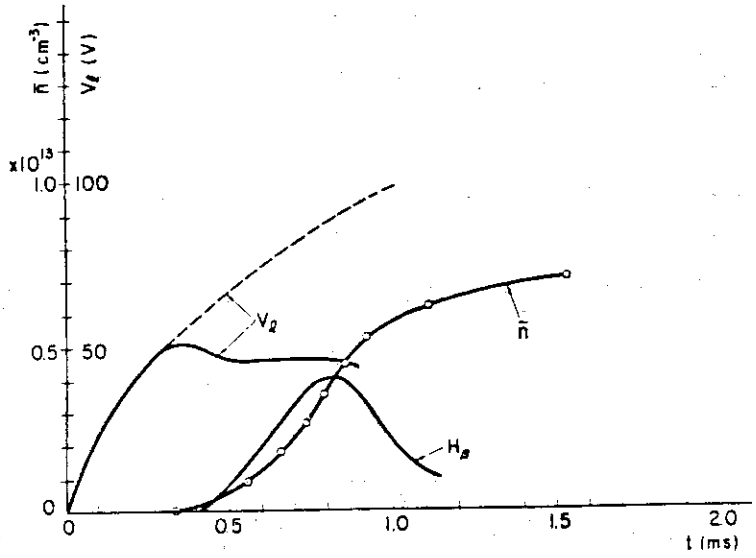

Fig. B.1 Time evolution of average line density $\bar{n}$, loop voltage and H intensity under the optimum condition

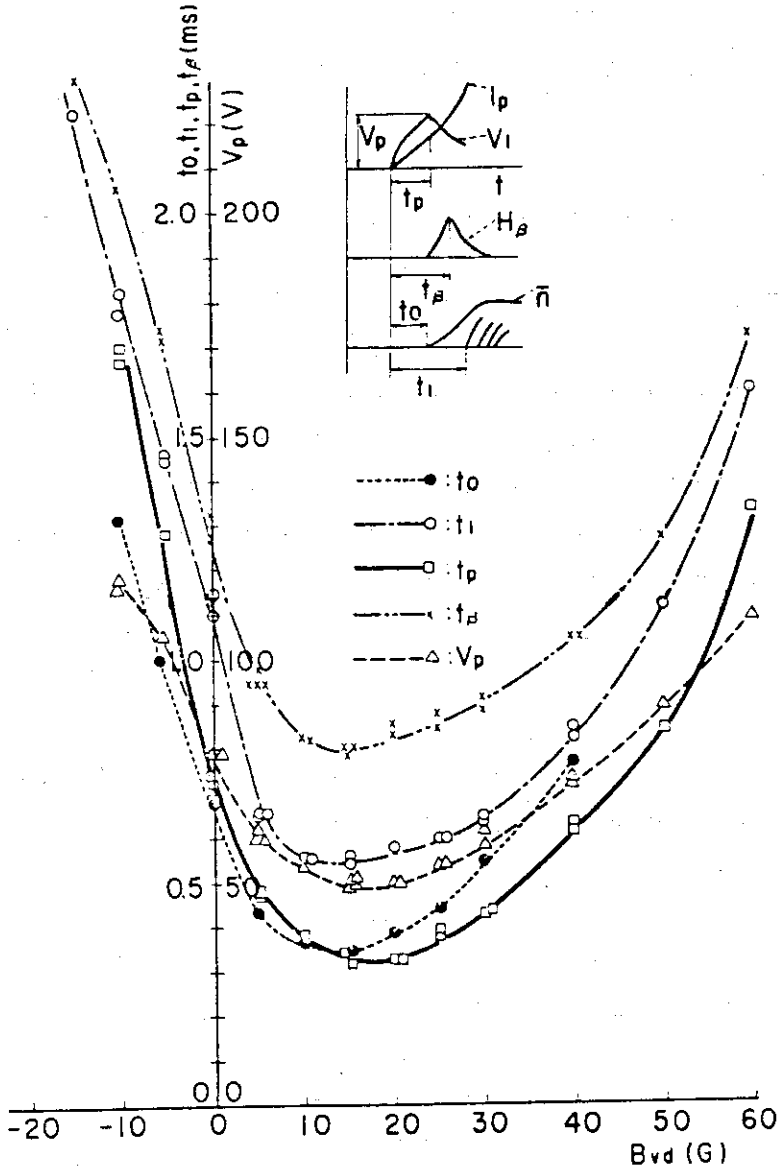

Fig. B.2 The dependence of the breakdown voltage and the time lag on the vertical field

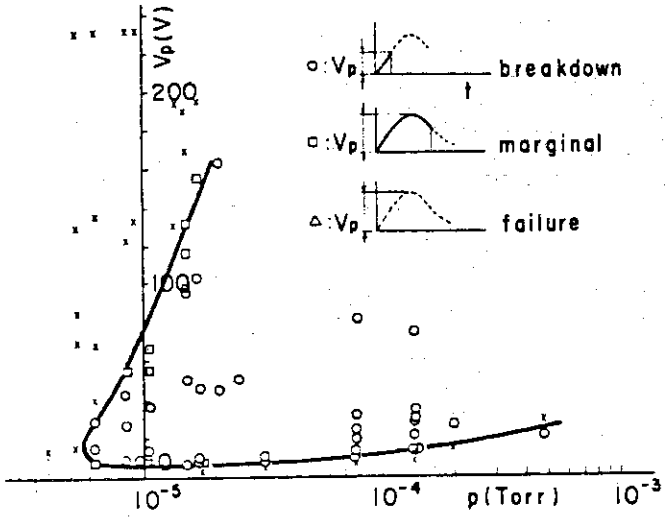

(a) B_h=15 G

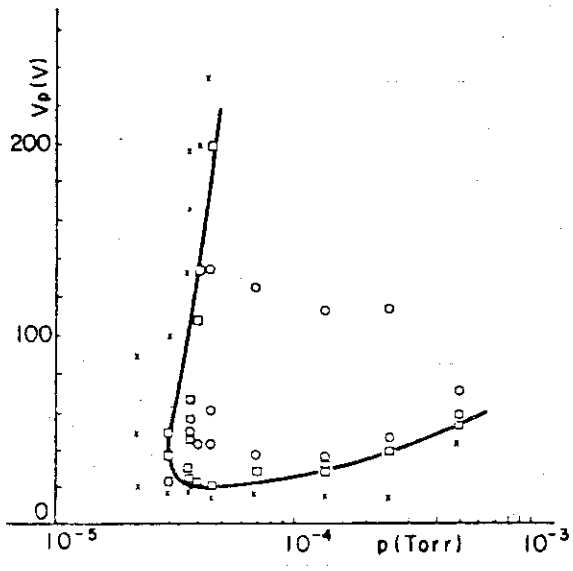

(b) B_h=0 G

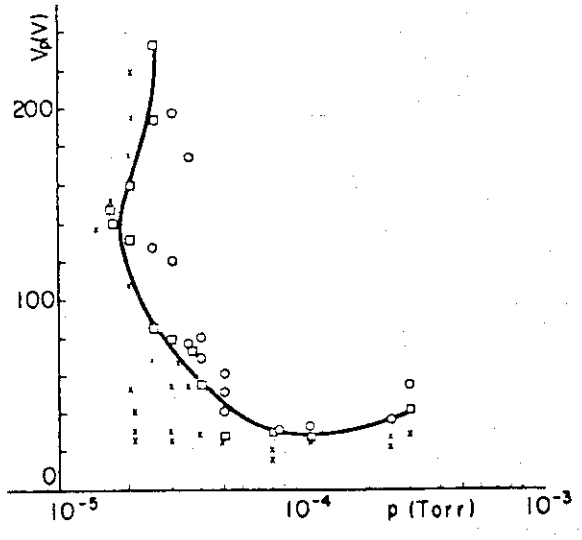

(c) B_h=30 G

Fig. B.3 V_p-p curve showing possible breakdown region with B_t=14 KG.

Vc=2KV

SHOT No 83313 P =7.8 x 10^{-5} TOrr

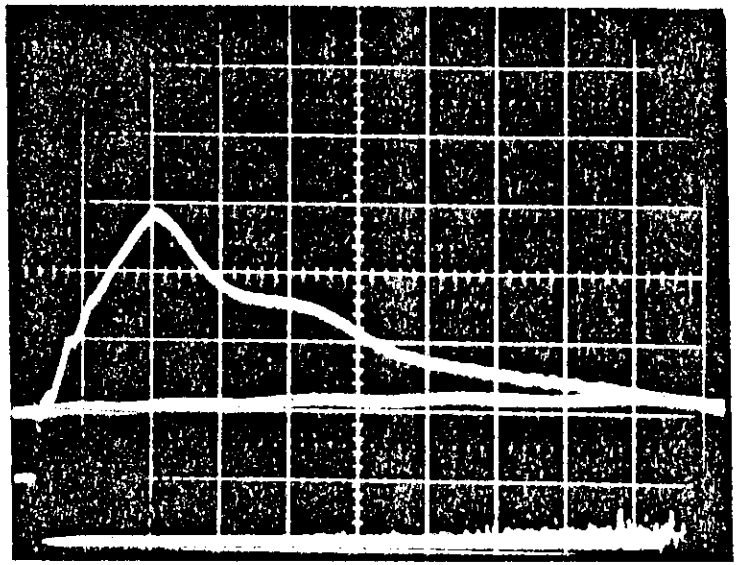

500μs/div.

Oneturn loop voltage 5v/div.

Plasma + linear Current 67.5KA/div.

Hard X ray

Fig. B.4 Oscilogram of oneturn loop voltage and current

SHOT No 83313

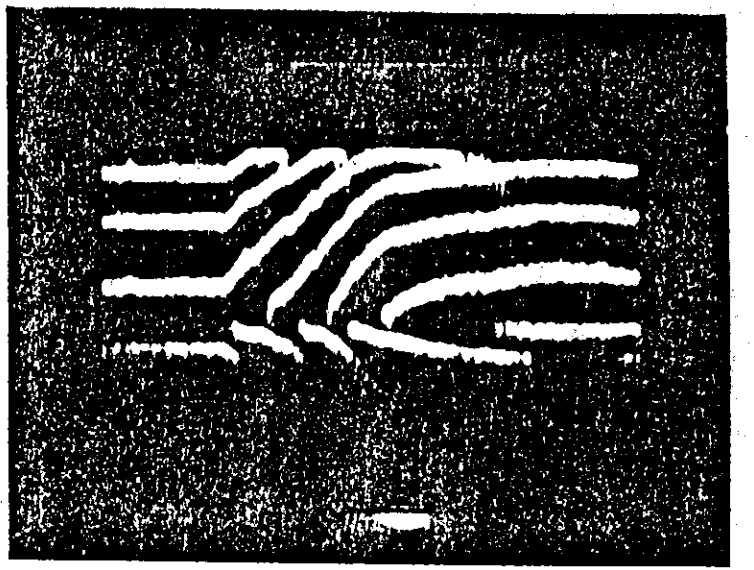

500μs/div.

1 fringe= 8.8 x 10^{11}/cc

4 mm micro wave int.

Fig. B.5 Zebra pattern showing electron density variation

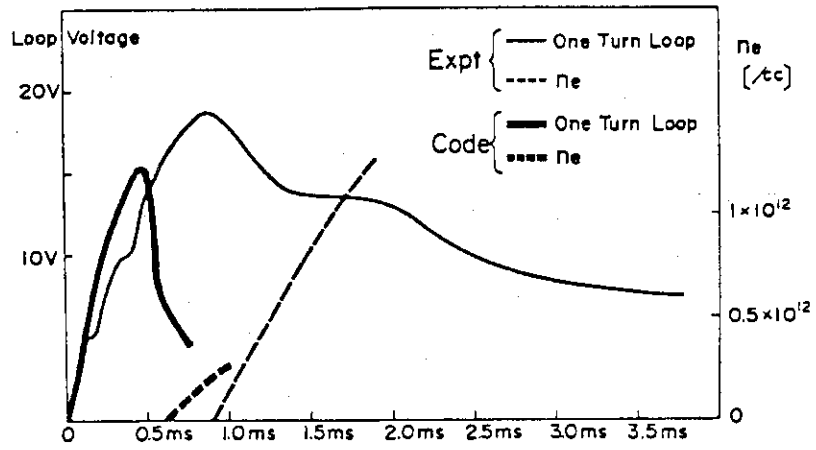

Fig. B.6 Comparison of experiment and calculation

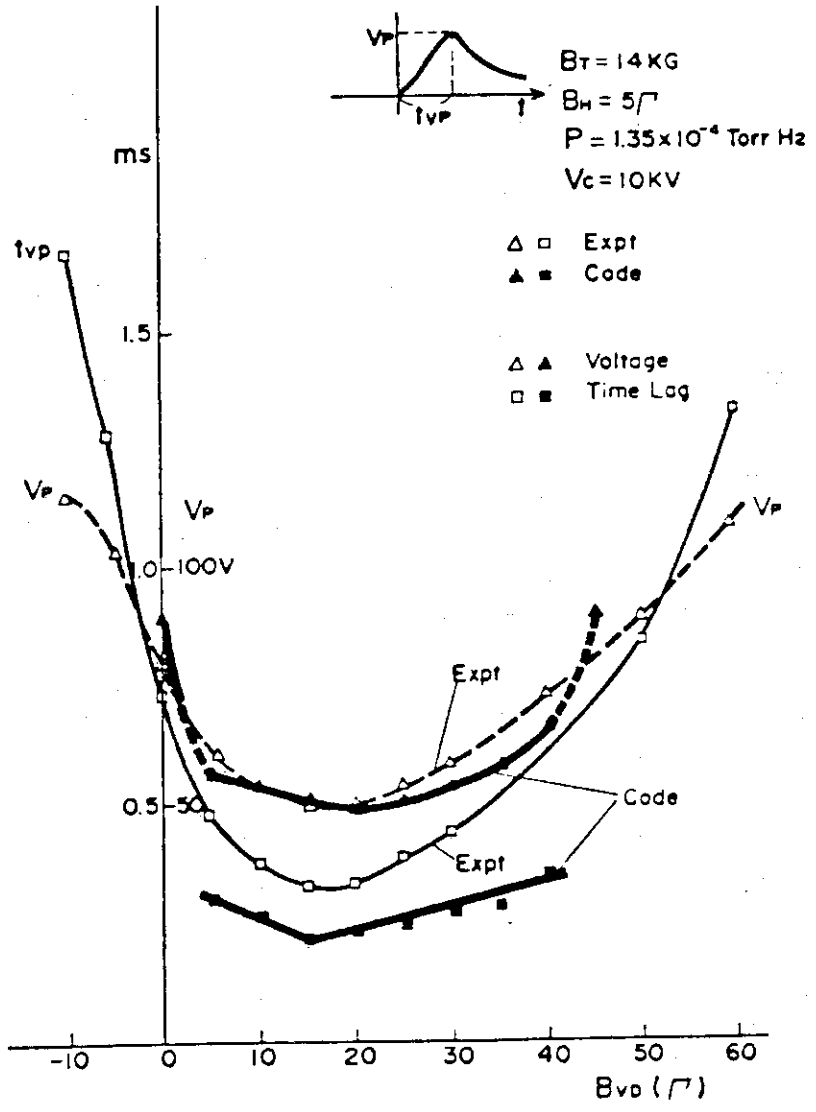

Fig. B.7 Variations of the breakdown voltage and time lag as a function of the vertical field B_{VD}. Expt indicates the experimental data of JFT-2 and Code the calculated values

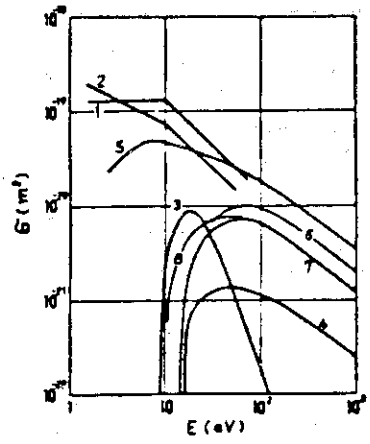

1. $e + H_2$
2. $e + H$
3. $e + H_2 \rightarrow e + 2H$
4. $e + H_2 \rightarrow e + H + H^*$
5. $e + H_2^+ \rightarrow e + H + H^+$
6. $e + H_2 \rightarrow 2e + H_2^+$
7. $e + H \rightarrow 2e + H^+$
8. $e + H \rightarrow e + H^*$

Fig. B.8 Electronic cross-sections

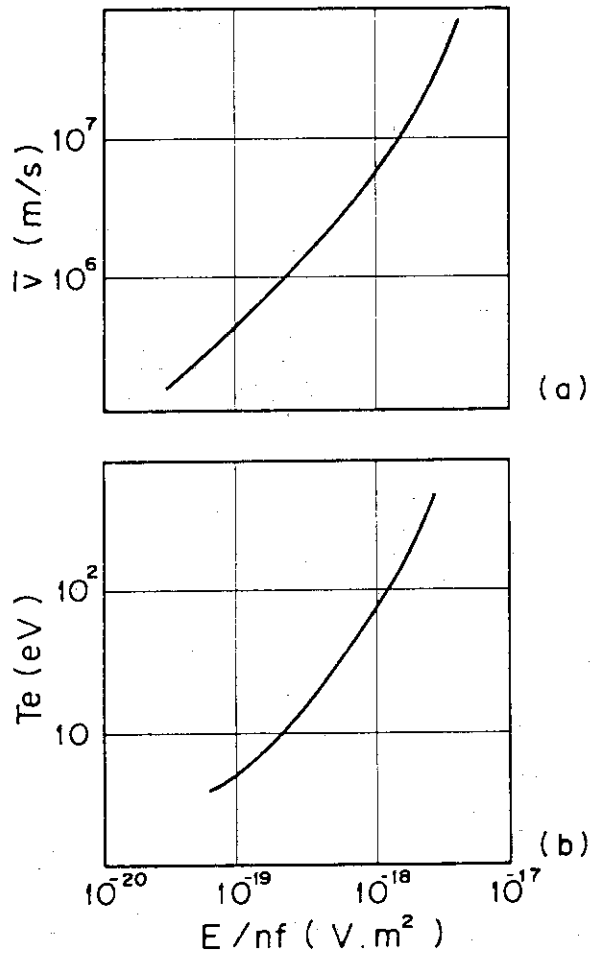

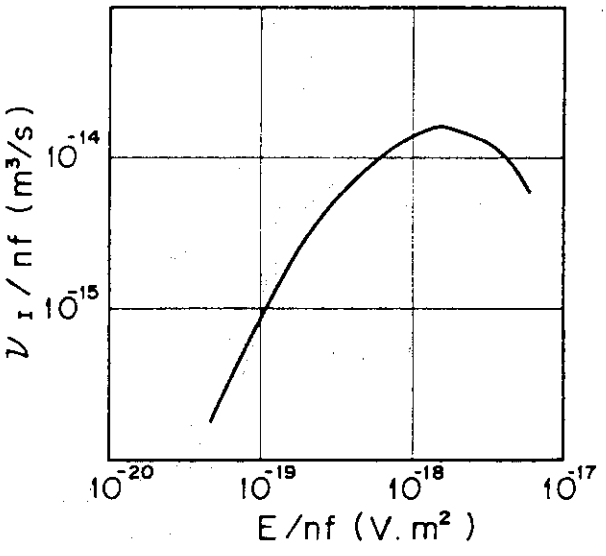

Fig. B.10 Ionization frequency

Fig. B.9 Electron drift velocity and electron temperature